biophysics COLAB

Curated Preprint
v2 • December 23, 2022
Peer Review Information

Reviewed Preprint
v1 • September 27, 2022

Activation-pathway transitions in human voltage-gated proton channels revealed by a non-canonical fluorescent amino acid

Esteban Suárez-Delgado, M. E. Orozco-Contreras, Gisela E. Rangel-Yescas, León D. Islas

Department of Physiology, School of Medicine, UNAM, Mexico City,04510, Mexico • Department of Biology, Xenon Pharmaceuticals Inc., 3650 Gilmore Way, Burnaby, BC V5G 4W8, Canada

Endorsement statement (22 December 2022)

The preprint by Suarez-Delgado *et al*. explores the mechanisms by which the Hv1 voltage-activated proton channel is dependent upon transmembrane voltage and pH by incorporating the small fluorescent non-canonical amino acid Anap into the S4 helix and monitoring its fluorescence. Anap spectra suggest the fluorophore resides in an aqueous environment and moves relative to a quenching aromatic residue (F150) in the S2 helix upon depolarization. Two kinetically distinct components of fluorescence change support the presence of at least three conformational states in the activation pathway of Hv1. Measurements using different pH gradients suggest that S4 movement and channel opening are similarly affected by pH gradients. This is the first study to incorporate Anap into Hv1, and provide a rigorous and thorough characterization of how the fluorophore can be used to explore mechanisms of gating and regulation, paving the way for future studies. The work will be of interest to physiologists and biophysicists investigating membrane protein mechanisms using non-canonical fluorescent amino acids.

(This endorsement by Biophysics Colab refers to version 2 of this preprint, which has been revised in response to peer review of version 1.)

Abstract

Voltage-dependent gating of the voltage-gated proton channels (H_V1) remains poorly understood, partly because of the difficulty of obtaining direct measurements of voltage sensor movement in the form of gating currents. To circumvent this problem, we have implemented patch-clamp fluorometry in combination with the incorporation of the fluorescent non-canonical amino acid Anap to monitor channel opening and movement of the S4 segment. Simultaneous recording of currents and fluorescence signals allows for direct correlation of these parameters and investigation of their dependence on voltage and the pH gradient (ΔpH). We present data that indicate that Anap incorporated in the S4 helix is quenched by an aromatic residue located in the S2 helix, and that motion of the S4 relative to this quencher is responsible for fluorescence increases upon depolarization. The kinetics of the fluorescence signal reveals the existence of a very slow transition in the deactivation

pathway, which seems to be singularly regulated by ΔpH. Our experiments also suggest that the voltage sensor can move after channel opening and that the absolute value of the pH can influence the channel opening step. These results shed light on the complexities of voltage-dependent opening of human H_V1 channels.

Significance statement

The activation mechanisms of voltage-gated proton channels (H_V1) are not well understood. Here we have combined patch-clamp fluorometry and a fluorescent non-canonical amino acid to uncover transitions in the activation pathway of human H_V1 that are modulated by voltage and the pH gradient.

Introduction

Voltage-gated, proton-permeable ion currents in a large variety of cell types and organisms are produced by the H_V1 gene (HVCN1 in humans), which encodes a membrane protein that is a member of the superfamily of voltage-sensing domains (VSDs) (Sasaki et al., 2006; Ramsey et al., 2006). These VSDs are also encountered in voltage-sensitive phosphatases (VSP) and voltage-gated ion channels (VGIC), and their principal function is to detect the membrane potential difference and translate it into a conformational change that activates VSP and opens VGIC (Catacuzzeno and Franciolini, 2022).

H_V1 is thought to form ion channels activated by voltage and employing a mechanism of activation similar to the VSDs of canonical voltage-gated potassium, sodium and calcium channels (Gonzalez et al., 2012). The functions of H_V1 channels are diverse, including intracellular pH regulation (Ma et al., 2022), charge compensation during immune response (Ramsey et al., 2009), modulation of flagellar beating in spermatozoa (Lishko and Kirichok, 2010), bioluminescence (Eckert and Sibaoka, 1968), and possible roles in calcification processes in marine organisms (Taylor et al., 2011; Rangel-Yescas et al., 2021). Also, H_V1 is involved in different pathologies such as B cell malignancy (Hondares et al., 2014), breast cancer (Wang et al., 2012), and post-ischemic brain injury (Wu, 2014; Yu et al., 2020); consequently, in recent years H_V1 has emerged as a possible pharmacological target (Zhao et al., 2018; Zhang et al., 2022).

Among all voltage-gated proton channels sequenced, the human orthologue, hH_V1, is the most widely studied (Musset et al., 2008). This channel is thought to be a functional dimer formed by two subunits comprising an intracellular N-terminus, a bundle of four transmembrane helices (TMH, S1-S4) in the VSD fold, and a long intracellular alpha helix that mediates a coiled-coil interaction, mainly responsible for dimerization and cooperative activation (Koch et al., 2008; Lee et al., 2008; Tombola et al., 2008). The fourth alpha helix, S4, contains positive charges represented by three arginine residues (R205, R208, and R211) in the characteristic VSD repeats. S4 is thought to undergo an outward displacement and rotation in response to depolarization, mostly in accordance to the helical screw rotation and displacement model of voltage-gating (Li et al., 2015). Unlike canonical VGIC, H_V1 lacks the two TMH that make up the pore region in canonical ion channels (S5 and S6); therefore, the VSD of H_V1 has a double function: it is responsible for detecting the electrical potential across the membrane and forming the pathway through which the protons will move once the channel is activated.

A characteristic of H_V1 activation is its dependence on the pH gradient or ΔpH (pH_o - pH_i). Native proton channels were first shown to open at more negative voltages when the proton gradient points in the outward direction (Cherny et al., 1995). It was shown that for every unit of ΔpH, the voltage of mid activation shifts ~40 mV. Subsequently, all native and cloned proton channels have

been found to approximately follow this rule (Sasaki et al., 2006; Ramsey et al., 2006; Rangel-Yescas et al., 2021; Musset et al., 2008; Smith et al., 2011; Zhao and Tombola, 2021). Recent experiments suggest that the proton gradient produces this effect by acting on the voltage sensor and not only affecting a close-to-open transition, since gating currents and channel opening are similarly modulated (Schladt and Berger, 2020; Carmona et al., 2021). However, the molecular mechanisms through which protons modulate voltage-sensor function are not known. Due to technical difficulties, such as not having a pore structure separate from VSD or the impossibility of patch-clamping without protons in the experiments, gating current recordings of H_V1 channels have been obtained from mutants of the *Ciona* H_V1 (ciH_V1) orthologue (Carmona et al., 2018, 2021) or mutants of human H_V1 (De La Rosa and Ramsey, 2018).

Patch-clamp Fluorometry (PCF) has been used to overcome these difficulties as a powerful tool that allows investigation of electrically silent conformational changes in VSDs associated with channel gating (Kusch and Zifarelli, 2014a), through following fluorescence intensity changes of a dye that generally is attached to the channel protein via chemical modification of cysteine residues or a fluorescent protein genetically encoded (Kusch and Zifarelli, 2014b). In ciH_V1 and hH_V1 proton channels, this technique has been employed to obtain evidence of cooperative gating, S1 movement during activation, and the pH sensitivity of S4 movement (Mony et al., 2015; Schladt and Berger, 2020; Qiu et al., 2013). As in other voltage-gated channels, these studies made use of the fluorophore tetramethylrhodamine (TMR), which was tethered to the S3-S4 linker, an extracellular-facing part of the channel (Cowgill and Chanda, 2019). While fluorophores like TMR have provided a means to observe conformational changes in many voltage-gated ion channels, including H_V1, due to their large size and cysteine reactive nature, they are difficult to incorporate in membrane-embedded portions of channels, without possible large perturbation of the protein fold or result in unspecific incorporation. For these reasons, incorporating a small fluorophore in the middle of transmembrane helices would be advantageous. Here, we exploit the small size, comparable to aromatic amino acids, of a genetically encoded fluorescent non-canonical amino acid, Anap (Chatterjee et al., 2013). By incorporating Anap at various positions in the S4 segment, we assess the conformational changes of the human voltage-gated proton channel (hH_V1) in response to voltage activation and pH modulation by performing patch-clamp fluorometry (PCF). We find our measurements can resolve a transition during the deactivation process that is strongly modulated by pH. Furthermore, we find that the changes in Anap fluorescence could be partially due to interaction with aromatic amino acids within H_V1.

Results

Incorporation of Anap into hH_V1

To study voltage-dependent transitions in a voltage sensor using patch-clamp fluorometry, it is desirable that the introduced fluorescent probe does not produce a major structural perturbation of the target protein. The relatively recently developed probe Anap (3-(6-acetylnaphtalen-2-ylamino)-2-aminopropanoic acid) is a small non-canonical fluorescent amino acid (Figure 1B), which has been shown to be easily genetically-encoded in proteins expressed in eukaryotic cells (Chatterjee et al., 2013; Puljung, 2021) Moreover, Anap has been successfully used as a reporter of voltage-dependent conformational changes (Kalstrup and Blunck, 2013) and as a FRET pair (Gordon et al., 2018) to probe ion channel dynamics. In this study, Anap was inserted into specific positions of the S4 segment of the human H_V1 proton channel (hH_V1) sequence (Figure 1A), with the purpose of examining its voltage and pH-dependent dynamics.

We selected the S4 helix as insertion target, since this region of the channel is proposed to undergo a voltage-dependent outward displacement that has been previously studied with different approaches, including voltage-clamp fluorometry (13-15).

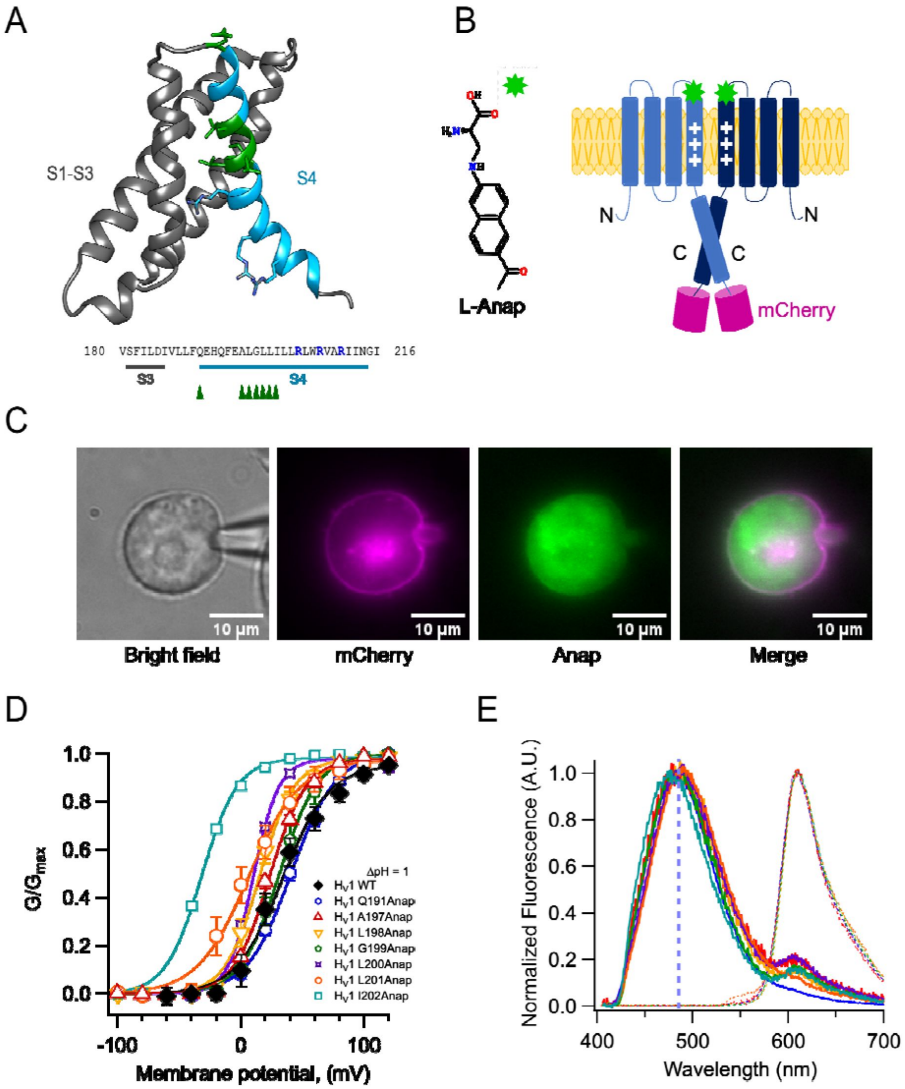

Figure 1.

Anap as a fluorescent probe in hH_V1. A) Ribbon representation of transmembrane segments S1-S4 of closed hH_V1 based on the model of Randolph et al. (Randolph et al., 2016). S1-S3 are in grey whereas S4 is in light blue. S4 positively charged arginine residues are shown as cyan sticks, whereas the residues where Anap was incorporated individually in the S4 segment are depicted as green sticks and with green arrow heads in the S3-S4 sequence below; positively charged arginine residues are indicated in marine blue. B) Structure of non-canonical amino acid Anap (left), and a schematic representation (right) that shows the incorporation of Anap (green star) into the hH_V1 dimer expressed in HEK293 cells. An mCherry fluorescent protein (magenta cylinder) was fused to the C-terminal end of hH_V1 as an Anap incorporation reporter. C) Images of a representative Patch-clamp Fluorometry (PCF) experiment, showing the voltage-clamped cell and the co-localization of Anap and mCherry fluorescence in the cell membrane for Anap incorporated at position Q191 of hH_V1. D) G-V curves obtained from currents produced by each hH_V1 mutant rescued by Anap incorporation. All G-V s were obtained at ΔpH=l and compared with hH_V1 WT. Continuous lines are the fit of the conductance data to equation 1; fit parameters are summarized in Supplemental table I. The incorporation of Anap at the 1202 site sifts the G-V ~65 mV to more negative potentials. Data shown are mean ± s.e.m. E) Normalized mean emission spectrum of Anap (continuous lines) and mCherry (dashed lines) at each incorporation site (color code from D) recorded at resting potential in non-patched cells. Q191(n=15); A197(n=8); L198(n=7); G199(n=6); L200(n=10); L201(n=30); I202(n=10). The vertical blue line indicates the peak emission of Anap in water (486 nm). A second emission peak can be distinguished in every position inside S4 where Anap was incorporated, except Q191Anap. This peak is located around 610 nm which coincides with the peak emission of mCherry.

We were able to successfully substitute amino acids by Anap at positions Q191 in the S3-S4 linker and A197, L198, G199, L200, L201, and I202 in the S4. Anap efficiently rescued expression of channels containing an amber stop codon (TAG) in the selected position, as judged both by appearance of red fluorescence produced by the mCherry fluorescent protein appended in the C-terminus (Figure 1C and Figure 1-supplement 1A) or the appearance of proton currents recorded from HEK 293 cells in the whole-cell patch-clamp configuration (Figure 1D, Figure 1-Supplement 2 and Supplementary Table I).

The substituted channels gave rise to voltage-activated currents, with similar range of activation to WT as judged by their conductance vs. voltage (G-V) curves (except I202Anap channels). Furthermore, that Anap was able to specifically rescue TAG-containing channels was demonstrated by control experiments in cells cotransfected with mutant channels and the pANAP plasmid in the absence of Anap, which showed absence or very small proton currents as compared to cells cultured in the presence of Anap (Figure 1-supplement 1B).The observed fluorescence emission spectrum of the Anap signal present in the membrane (Figure 1C), which presumably originates mostly from Anap incorporated into channels, shows that there are no major or systematic variations on the peak emission wavelength (Figure 1E). The peak emission wavelength for all positions varies, but is near 485 nm, except the most C-terminal and presumably deepest position, I202Anap, which is 477 nm (Figure 1-Supplement 3A). This result suggests that the local environment of Anap in these positions, except 202Anap, is very similar and consistent with a mostly polar environment since the peak emission of Anap in aqueous solution is ~486 nm.

Figure 1E also shows that the emission spectra of positions other than Q191Anap exhibit a small extra peak near 610 nm, that corresponds to the peak emission of mCherry. Since the excitation peak of mCherry is 587 nm (Shaner et al., 2004), we performed experiments with hH_V1-mCherry channels to measure direct mCherry excitation by our 405 nm laser. The results indicate that this peak is mostly produced by direct excitation of mCherry at 405 nm (Figure 1-Supplement 3B).

Insensitivity of Anap to pH

In order to use Anap as a reporter of conformational changes in H_V1 proton channels, and given that these channels are able to change the pH of the surrounding solution (De-la-Rosa et al., 2016; Zhang et al., 2016), we first wanted to validate if this fluorophore is insensitive to pH changes. The amino acid form of Anap that we use is the methyl-ester, which contains amino and carboxy groups. The fluorescence of methyl-ester Anap could be affected by protonation because it could alter electron distribution, for this reason, we reasoned that the best assay to test the pH dependence of Anap fluorescence is to use already incorporated Anap. For this purpose, we used the mutant Q191Anap, which incorporates Anap in the S3-S4 loop, which faces the extracellular solution, even in the deactivated state of the channel (Figure 1A). Since the emission spectrum of Q191Anap channels was measured from non-voltage clamped transfected HEK cells, fluorescence was obtained only from membrane regions to assure that the signal comes mostly from channels exposed to the extracellular solution changes and not channels in intracellular compartments, which will not be exposed to the pH changes.

To ensure that most of the fluorescence is collected from channels in the membrane, the membrane region was identified by the fluorescence of mCherry-containing channels that clearly delineates it (Figure 2-Supplement 1). Spectra were then collected only from this small region of membrane.

These measurements showed that the fluorescence of channel-incorporated Anap is not significantly changed in intensity or shape of the emission spectrum over the pH range 3 to 9 (Figure 2A and B), indicating that this fluorophore is insensitive to pH and that Anap fluorescence should not be affected by local pH changes, which might be produced as a consequence of proton currents.

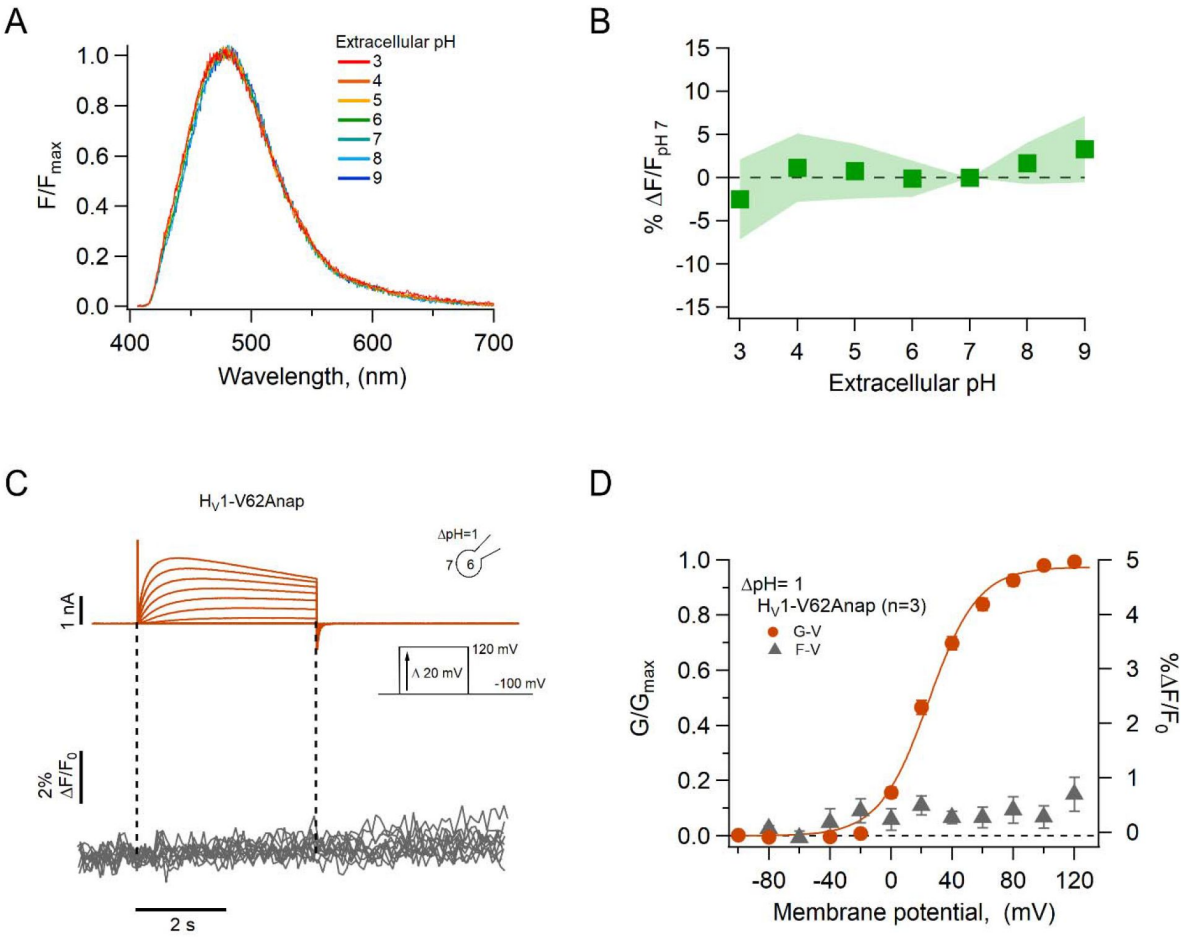

Figure 2.

The fluorescence of incorporated Anap is stable to external acidity and local pH changes. A) Mean spectra of Anap fluorescence in the hH_V1-Q191Anap mutant at each external pH tested (pH_o) recorded at the resting potential in non-patched cells. The emission peak of spectra of Anap remained inside the wavelength range of 475-480 nm. B) Percentage of fluorescence intensity change normalized to fluorescence at pH_o 7 in hH_V1-Q191Anap mutant (n=13). The intensity was measured from the peak of emission spectra. C) Representative PCF experiments with the hH_V1-V62Anap mutant. Currents (upper panel, orange traces) and fluorescent signal (lower panel, gray traces) were elicited in response to voltage pulses from −100 mV to 120 mV in steps of 20 mV. D) F-V and G-V relationships from the experiments shown in C. Relative fluorescence changes at the end of voltage test pulses are shown in gray triangles, and conductance is shown in orange circles. The orange continuous line is the fit to equation 1 of G-V data (fit parameters: $V_{0.5}$ = 24.4 ± 1.6 mV; q = 1.5 ± 0.1 e_0)· Data in B and D are Mean ± s.e.m.

As a further test of our data showing pH-insensitivity of channel-incorporated Anap and to validate the use of Anap in proton channels, we incorporated the amino acid in a position at the N-terminus of the channel, V62Anap. This amino acid is located in the intracellular part of the channel and should be subject to changes in local internal pH during channel activation (De-la-Rosa et al., 2016) but not show changes in fluorescence as a function of voltage-dependent conformational changes. As expected, we did not detect Anap fluorescence changes, although the amino acid was incorporated into functional channels, as judged from proton currents recorded simultaneously with fluorescence (Figure 2C and D). This result further supports the use of Anap in voltage-gated proton channels to measure conformational changes.

Voltage-dependent changes of Anap fluorescence

Previous experiments in which other dyes like tetra-methyl-rhodamine maleimide (TMRM) were used to label cysteine residues located in the amino-end of the S4 segment of voltage-sensing domains, including the *Ciona* and human H_V1 channels (Schladt and Berger, 2020; Mony et al., 2015; Qiu et al., 2013), usually result in fluorescence signals that are reduced upon depolarization by a voltage-dependent quenching process (Vaid et al., 2008; Cha and Bezanilla, 1998). In contrast, when we incorporate Anap at position A197, located towards the extracellular end of the S4, depolarization induced an increase of the fluorescence, along with proton currents. The fluorescence increase saturates at depolarized voltages, suggesting that it is produced by a saturable process such as voltage-sensor activation. The direction of this fluorescence change is the same when measured at a ΔpH of 0 or 2, suggesting the same conformational change in the S4 voltage sensor occurs at different pH gradients, albeit over a different range of voltages (Figure 3A and B).

We compared the kinetics of current and fluorescence by fitting an exponential function to the second half of the signal time course and plotted the time constant as a function of voltage (Figure 3C). Both current and fluorescence have the same voltage dependence, but the current is ~1.3 times faster than the fluorescence. Although not a very large difference, this can be explained by an overestimation of the current time course due to slight proton depletion observed with large currents.

When F-V and G-V curves are plotted together, it is evident that sensor movement paralleled the activation of the proton conductance. At three different values of the pH gradient (ΔpH 0, 1 and 2), both the F-V and G-V curves are almost superimposable and shift along the voltage axis by the same amount of ~40 mV/pH unit (Figure 3D), which is expected of H_V1 channels (Cherny et al., 1995). Only at ΔpH = 2 the fluorescence signal is shifted to slightly more negative voltages than the conductance and only at voltages at which channel activation begins. The observed voltage shift of the G-V is ~31 mV from ΔpH 2 to 1 and ~43 mV from ΔpH 1 to 0 and is very similar for the F-V curves. This result indicates that the ΔpH-dependence of gating is preserved in channels with incorporated Anap, and that the voltage sensor movement occurs in the same voltage range as the formation of the proton permeation pathway.

Anap is an environmentally sensitive dye, which shifts its emission to red wavelengths in increasingly polar solvents (Figure 3-Supplement 1). To understand the origin of the increased fluorescence observed during activation, we measured the emission spectra of A197Anap in voltage-clamped cells at different voltages. Fluorescence was measured from channels in the membrane region, which are identified by the mCherry signal, similar to Figure 1C. Figure 3E plots the spectra obtained at voltages ranging from −100 to 140 mV and it shows that the fluorescence increases with depolarization and has the same voltage-dependence as the fluorescence measured in Figure 3A, B and C at the same ΔpH (Figure 3E, inset). On the other hand, the peak emission wavelength remains the same at negative or positive voltages, indicating that the increase in fluorescence is not due to depolarization-driven wavelength shifts

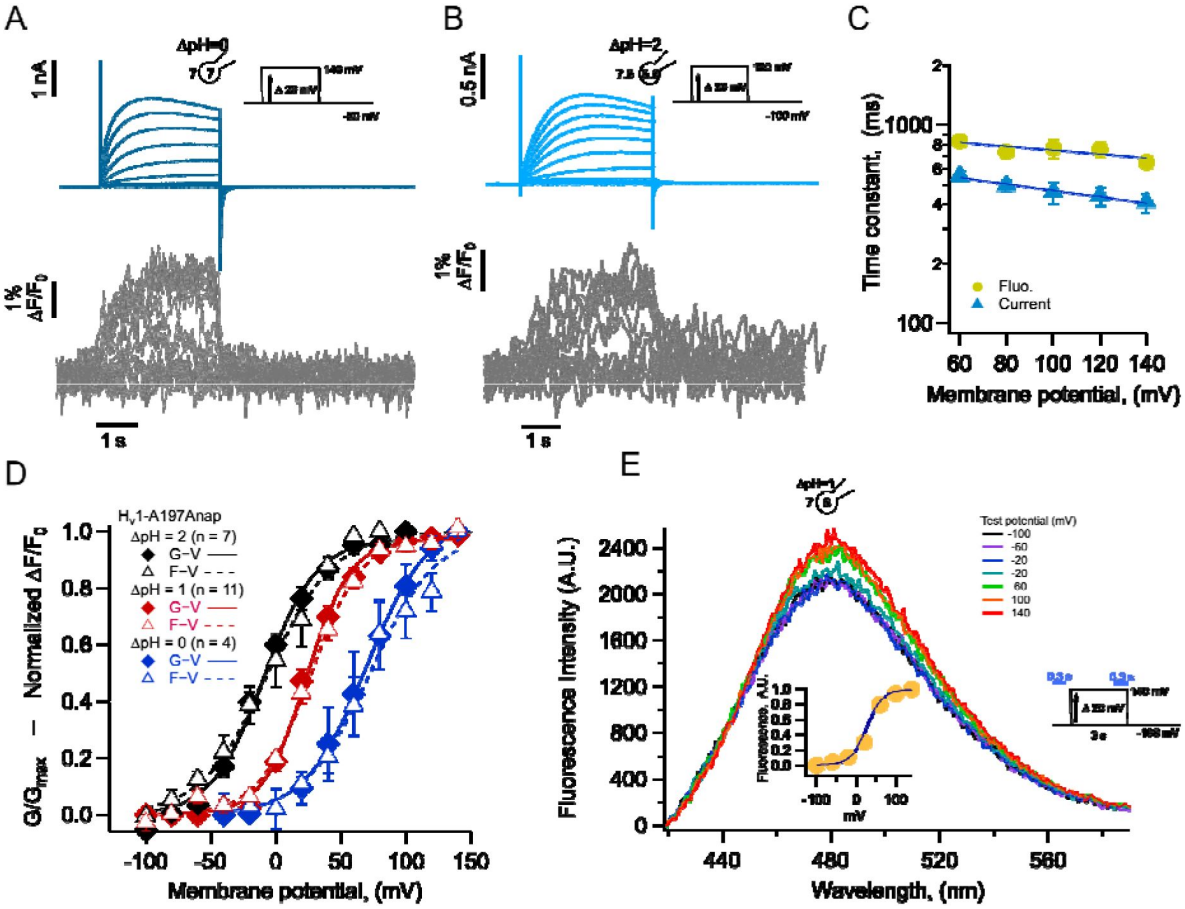

Figure 3.

Anap incorporation in position A197 reveals that the movement of S4 is modulated by ΔpH. A-B) Representative PCF experiment with A197Anap at ΔpH=0 and ΔpH=2, respectively. Proton current families (upper panels) are shown in blue traces and fluorescent Anap signal (lower panel) in gray traces. C) Activation time constant of current (blue) and fluorescent (lemon) signals at ΔpH=0 obtained by fitting Eq. 3. The dark blue curve shows the exponential fit to Eq. 4. The fit parameters were: $\tau(0)$ = 935 ms and q = −0.06 e_0 for fluorescence and 678 ms and −0.09 e_0 for current. D) F-V (empty triangles) and G-V (filled diamonds) curves and different ΔpH values (ΔpH=0 in blue; ΔpH=1 in red; ΔpH=2 in black). The data were fit to equation 1 (G-V, continuous curves; F-V, discontinuous curves) with the following parameters: ΔpH=0; F-V: $V_{0.5}$ = 72.3 ± 6 mV; q = 1.0 ± 0.1 e_0. G-V: $V_{0.5}$ = 69.6 ± 1.5 mV; q = 1.1 ± 0.1 e_0. ΔpH =1; F-V: $V_{0.5}$ = 26.6 ± 1.5 mV; q = 1.3± 0.1 e_0. G-V: $V_{0.5}$ = 23.4 ± 1.3 mV; q = 1.5 ± 0.1 e_0. ΔpH = 2; F-V: $V_{0.5}$ = −6.1 ± 1.8 mV; q = 1.0 ± 0.1 e_0. G-V: V0.5 = −9.2 ± 2.3 mV; q = 1.2 ± 2.4 e_0. E) Emission spectra of Anap in the A197Anap mutant obtained in steady-state (300 ms at the end of holding potential and the end of the test pulse, green bars in the inset) in response to different voltages (color code indicates the test pulse in mV: purple, −60; dark blue, −40; light blue, 20; cyan, 0; light green, 20; dark green, 40; olive, 60; yellow, 80; orange, 100; dark red, 120; red, 140). The inset plots the amplitude of the emission peak as a function of test voltage. The smooth curve is the fit of the fluorescence data at ΔpH=1 shown in panel D. Summary data shown in C and D are mean ± s.e.m.

of the emission spectra. We interpret this result as an indication that Anap incorporated at position A197 remains in a polar environment at all voltages or that small changes in polarity change the quantum yield of Anap but not the emission spectrum.

H_V1-197Anap is quenched by a phenylalanine in the S2

The increase of the Anap fluorescence at position 197 in the S4 seen with depolarization could be interpreted as a reflection of an outward movement of the S4 and exposure of Anap to a more polar environment (Figure 3 -Supplement 1), that in principle will produce a red shift of the emission spectrum and an increase of the fluorescence that is detected. However, as shown in Figure 3E, the shape of emission spectrum of Anap remains unchanged at all voltages and with a constant emission peak at ~480 nm, indicating that the fluorophore remains in a polar environment in the closed and open states and thus, a change in local polarity is likely not the principal cause of dequenching.

Many fluorophores can be quenched by aromatic amino acids through mechanisms such as π-stacking or photoinduced electron transfer, both mechanisms require close proximity (Islas and Zagotta, 2006; Klymchenko, 2017; Pantazis and Olcese, 2012; Young and Artigas, 2021). Evidence for the existence of a quenching group near Anap incorporated in the S4 can be obtained from examination of the ratio of fluorescence of Anap and mCherry in channels as a function of its position along the S4 (Figure 4-Supplement 1). This analysis shows that for positions deeper into the S4 segment, the Anap/mCherry ratio diminishes, suggesting that in those sites Anap is closer to a quenching group.

For these reasons, it is conceivable that the Anap quencher in H_V1, could be an aromatic residue located near the introduced fluorophore in the closed state and upon S4 movement, increases its distance, generating the observed dequenching. We used a structural model of H_V1 derived from experimental data (Randolph et al., 2016) and replaced A197 with Anap. Figure 4A shows Anap in salmon-colored spheres and highlights aromatic residues within the transmembrane domains of a monomer as dotted spheres. A possible candidate for an Anap quencher is F150 (yellow spheres), because this residue is the closest aromatic to Anap that is not in the S4 and F150 will presumably remain in its position as 197Anap undergoes an outward displacement with depolarization. In contrast, other aromatic residues which are closer to 197Anap and are part of the S4, will presumably move with all the S4 as a rigid body. Incidentally, an equivalent phenylalanine to F150 has been identified as the charge transfer center in canonical voltage-gated potassium channels and in H_V1 (Tao et al., 2010; Hong et al., 2013).

To test this hypothesis, we made the double mutant F150A-A197Anap and estimated the relative amount of basal Anap quenching, by comparing the emission spectra of both Anap and mCherry in the same membrane region. Figures 4B and C shows that the double mutant displays a significantly increased Anap fluorescence (~60 %) relative to mCherry, when compared to A197Anap alone, suggesting that indeed, phenylalanine 150 is capable of quenching Anap in the closed state (at the resting potential of HEK cells of −20 to −40 mV (Thomas and Smart, 2005b) and at the employed ΔpH ~ −0.2 (pH_o = 7) most channels should be in the closed state).

Despite having removed the quenching group, F150A-A197Anap channels still show voltage-dependent fluorescence changes (Figure 4D), suggesting the presence of additional quenchers or that in the absence of F150, Anap at 197 becomes sensitive to polarity changes.

The voltage dependence of the fluorescence signals from F150A-A197Anap channels shows significant differences from those of A197Anap alone (Figure 4E). At values of ΔpH of 0 and 1, fluorescence precedes the increase in conductance, indicating that the conformational change of

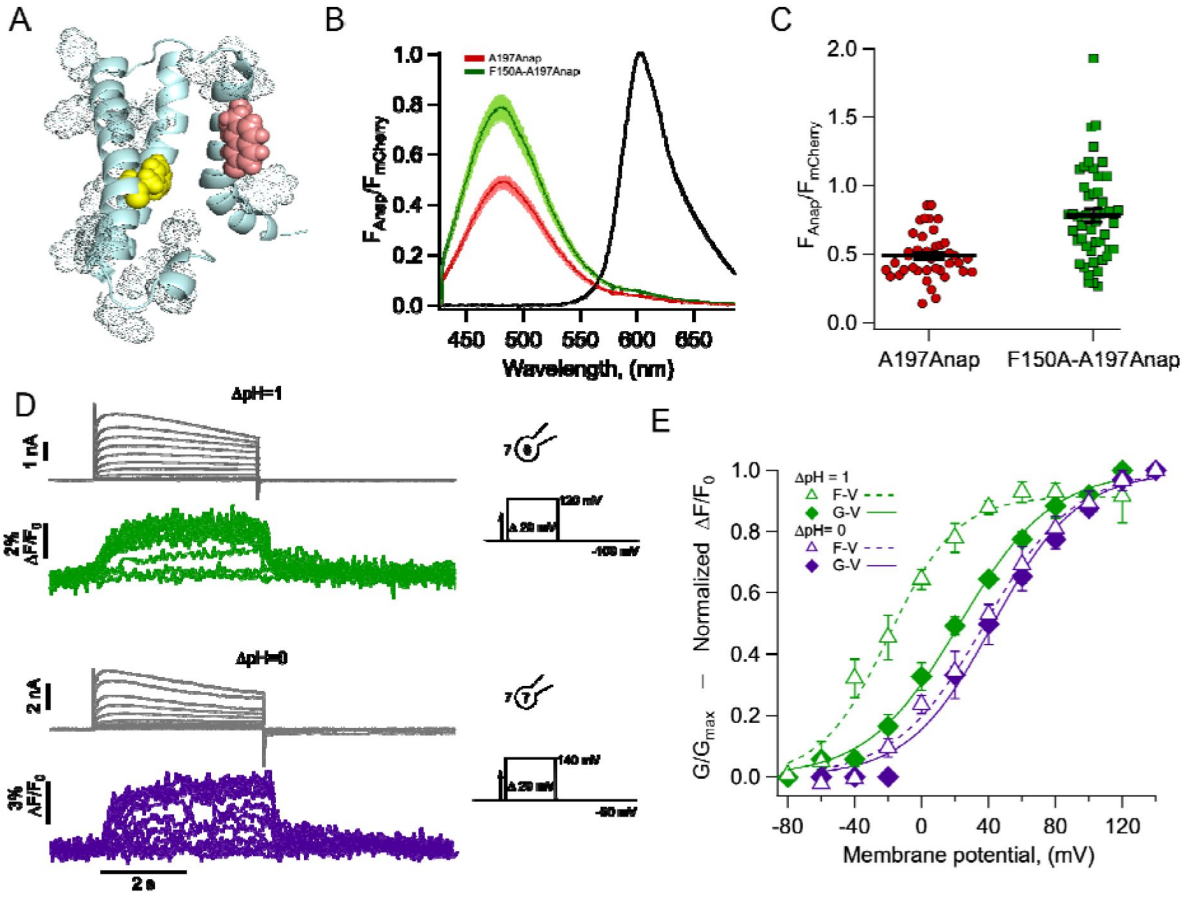

Figure 4.

The charge transfer center (F150) is an Anap quencher. A) Cartoon showing the presence of aromatic residues in hH_V1 (rendered as space-filling dots, main chain in light blue, S3 was removed for illustration). F150 in yellow and Anap in pink. B) Averages of spectra of Anap incorporated in both mutants (H_V1-A197Anap, red; H_V1-F150A-A197Anap, green) normalized to the fluorescence of mCherry (black). Spectra were obtained at the resting potential in non-patched cells. The double mutant's brightness is approximately 60% higher. Shadows represent s.e.m. C) Comparison of the intensity of the emission spectrum peak of Anap normalized to the intensity of the fluorescent protein mCherry between the mutant H_V1-A197Anap-Cherry (0.49 ± 0.03) and double mutant H_V1-FI50A-A197Anap-Cherry (0.79 ± 0.05), taken at 48 hours post-transfection. Each point indicates an individual spectrum measured from a single cell; n = 41 and 49, respectively. Black horizontal lines are the mean ± s.e.m. T-test value p <0.001. D) Representative current and fluorescence traces from PCF experiments of the double mutant H_V1-F150A-A197Anap at ΔpH=1 (upper panel) and ΔpH=0 (lower panel). E) Comparison of G-V (diamonds) and F-V (triangles) relationship between both ΔpH conditions (ΔpH=1 in green; ΔpH=0 in purple) of the double mutant H_V1-F150A-A197Anap. F-V curve of H_V1-F150A-A197Anap at ΔpH=0 is shifted negatively around 58 mV compared to ΔpH=1. Boltzmann fit parameters of H_V1-F150A-A197Anap were: ΔpH=l F-V: $V_{0.5}$=−19.8 ± 2.7 mV; q =1.2 ± 0.1 e_0; G-V: $V_{0.5}$ = 22.7 ± 2.3 mV; q = 0.9 ± 0.1 e_0. ΔpH=0 F-V: $V_{0.5}$=38.0 ± 3.0 mV; q =0.9 ± 0.1 e_0; G-V: $V_{0.5}$ = 42.6 ± 3.8 mV; q = 1.0 ± 0.1 e_0. Data shown in B, C and E are mean ± s.e.m.

the S4 segment occurs at more negative voltages than the formation of the proton-permeable pathway. This effect is more pronounced at ΔpH = 1. Interestingly, the difference of $V_{0.5}$ of the F-V curve between ΔpH= 0 and 1 is ~58 mV, similar for A197Anap, which is ~46 mV.

A distinct gating transition detected by Anap fluorescence

The fluorescence time course of the F150A-A197Anap channels shows an interesting characteristic; the OFF signals (F_{off}) that are produced at the return of the voltage to the holding potential and represent the return of the voltage sensor to the resting states, show a two-component kinetic behavior. This is particularly evident at ΔpH = 0 (Figure 4D), where F_{off} shows a very rapid quenching followed by a much slower component, suggesting that the voltage sensor can move back to its resting position at varying rates.

To explore the kinetics of fluorescence signals during repolarization, and since this double mutant removes a quenching group, we used the hH_V1-201Anap channels. We reasoned that this mutant channel, which has Anap in a deeper position in the S4 and presumably closer to F150 in the closed state, might be a better reporter of the kinetics of S4 movement.

Figures 5A, B and C show simultaneous current and fluorescence recordings from hH_V1-1201Anap channels at three different ΔpH values of 0, 1 and 2. As with the hH_V1-A197Anap construct, the voltage-dependence of the conductance and fluorescence are almost superimposable and shows a large shift of >40 mV/pH unit (Figure 5D).

The most remarkable feature of these fluorescence traces is that, at ΔpH = 0, the OFF signal during repolarization (F_{off}) has two distinct kinetic components. The deactivation tail currents at −60 mV decay exponentially, with a time constant of 141 ±55 ms, while the F_{off} can be fit to a sum of two exponentials with time constants of 129 ± 68 ms and 8.6 ± 0.74 s. (Figure 5-Supplement 1). The presence of the two components in F_{off} suggest that the return of the voltage sensor to its resting state can occur at varying rates. In particular, the slow component is consistent with the immobilization of the off-gating charge observed in monomeric *Ciona* H_V1 channels (Carmona et al., 2018). The slow off-component is also present at ΔpH = 1 and 2, although its amplitude is smaller. We did not undertake a systematic kinetic analysis of current and fluorescence traces during channel activation due to the alterations that proton depletion cause on the current time course, especially for the larger currents observed at ΔpH = 2.

Instead, to qualitatively understand the kinetics of the fluorescence signals, we used a simplified kinetic model of channel activation (Scheme I), similar to a model that was previously used to study the voltage-dependent kinetics of hH_V1 (Villalba-Galea, 2014).

$$C_0 \underset{k_{10}}{\overset{k_{01}}{\rightleftharpoons}} C_1 \underset{k_{21}}{\overset{k_{12}}{\rightleftharpoons}} C_2 \underset{k_{32}}{\overset{k_{23}}{\rightleftharpoons}} O_3 \qquad \text{Scheme I}$$

In this model, one of the backward transitions (k_{21}) between closed states is set to be much slower than the open to closed transition (O_3->C_2), resulting in a large difference between the closing kinetics of the ionic current, mostly determined by k_{32}, and the fluorescence signals. This kinetic difference can account for the biphasic behavior of the F_{off} signal, and especially the slow component of its time course (Figure 5E). The model also indicates that when the internal pH is lower than the external pH (ΔpH=2), this slow rate constant is more affected than any other, indicating a conformational step that is especially sensitive to pH.

While the simple model in Scheme I can account qualitatively for the observed kinetics of 201Anap channels, the experimental F-V relationship is superimposable on the G-V curve (ΔpH=0 and 1) or positively shifted by ~10 mV (ΔpH=2) with respect to the G-V curve, which is not a feature predicted by Scheme I and is reminiscent of channels that can open to multiple open states,

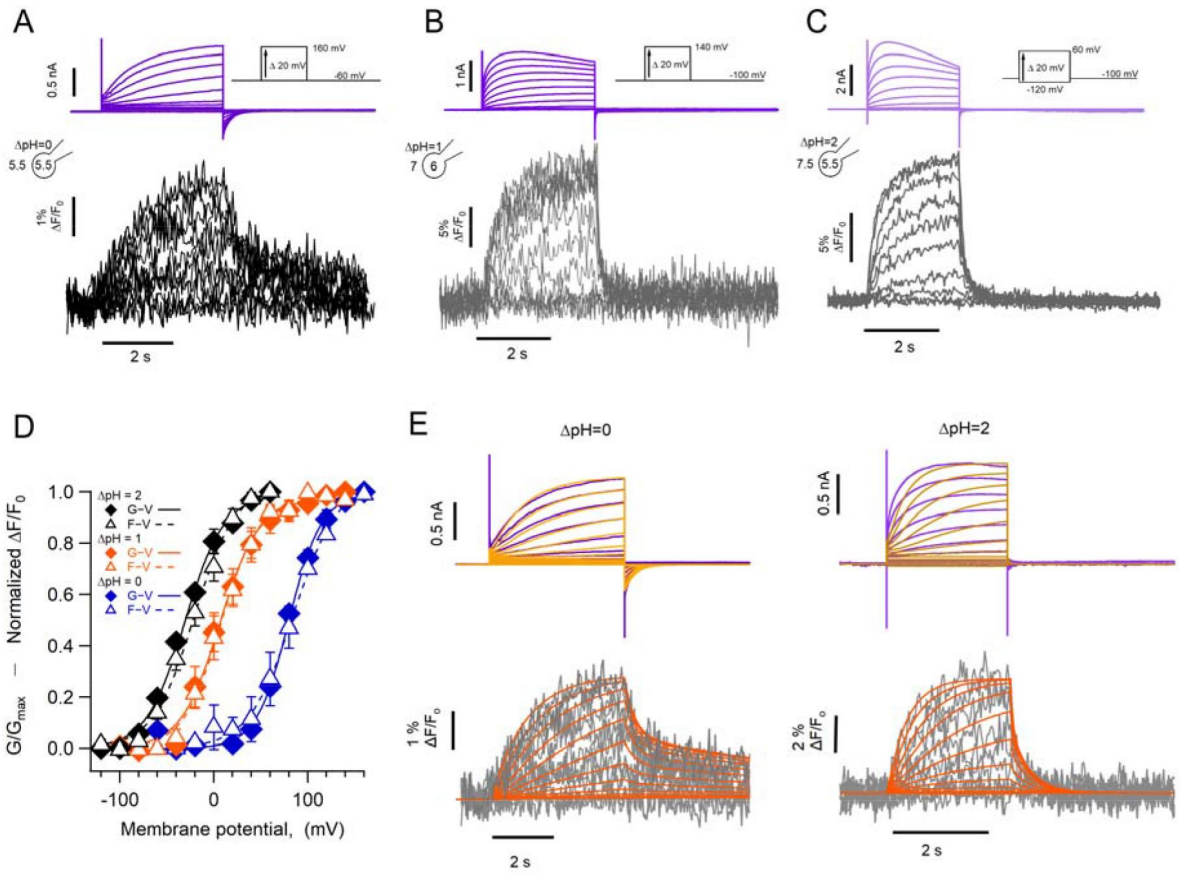

Figure 5.

The kinetics of fluorescent signal during deactivation is strongly modulated by pH. Representative PCF experiments with the hH_V1-L201Anap mutant at: A) ΔpH=0. B) ΔpH=1. C) ΔpH=2. Current families are shown in the upper panel (purple traces) and fluorescent signals in the lower panel (black and gray traces). D) G-V (filled diamonds) and F-V (empty triangles) relationships at ΔpH=0 (blue markers, n = 3), ΔpH=1 (orange markers, n=4) and ΔpH=2 (black markers, n=5) of mutant hH_V1-1201Anap. Data are mean ± s.e.m. Note that the difference between the activation at ΔpH=1 and ΔpH=0 is around 77 mV/ΔpH unit. Boltzmann fit parameters: ΔpH=0, F-V; $V_{0.5}$= 84.6 ± 2.1 mV, q =1.0 e_0 ± 0.1. GV; $V_{0.5}$= 79.7 ± 1.8 mV, q = 1.4 ± 0.1 e_0. ΔpH =1, F-V; $V_{0.5}$= 7.7 ± 1.6 mV, q =1.2 ± 0.1 e_0. G-V: $V_{0.5}$= 6.3 ± 2.2 mV; q = 1.2 ± 0.1 e_0. ΔpH = 2, F-V: $V_{0.5}$= −21.1 ± 2.3 mV; q =1.1 ± 0.1 e_0. G-V: $V_{0.5}$= −30.7 ± 1.9 mV; q = 1.2 ± 0.1 e_0. E) Comparison of the current and fluorescence at two values of ΔpH with the predictions of the sequential activation model in Scheme I.

Experimental current and fluorescence traces are color coded as in A). Simulated current traces are mustard colored and fluorescence traces are orange. Simulation parameters can be found in Supplementary Table II.

without the need of full voltage sensor activation (Stefani et al., 1997). This observation suggests that hH_V1 channels operate via a more complicated mechanism that the sequential gating illustrated by Scheme I, which might include channel opening before complete voltage-sensor movement. We tested a simple version of such an allosteric model and show that it can account, at least qualitatively, for current and fluorescence kinetics and for the relationships between G-V and F-V curves at varying ΔpH (Figure 5-Supplement 2). Interestingly, in this model the slow deactivation rate constant is also the step with the most sensitivity to pH (Supplementary Table III).

Absolute pH values are determinants of voltage sensor movement

One of the most intriguing characteristics of H_V1 channel gating, is its steep modulation by the pH gradient. While it has been shown that this modulation depends on the value of ΔpH, regardless of how it is set up (Cherny et al., 1995), there is evidence that the absolute value of pH can also exert an effect on gating (Cherny et al., 2015). In most of our experiments, the pH gradient was set up with a low value of intracellular pH, between 5.5 and 6.0. To test the effect of absolute pH, we carried out experiments with the same ΔpH of 0, with symmetric low ($5.5_{/}5.5$) or high ($7_{/}7$) intra/extracellular pH. The expectation was that, if pH gating of hH_V1 depends only on the pH gradient, the voltage sensor should move with essentially the same characteristics. Surprisingly, the fluorescence signals display important differences, as do the proton currents. Our results in Figure 6 show that when compared to ΔpH = 0 ($5.5_{/}5.5$), the fluorescence in symmetric pH_o and pH_i = 7.0 has a rapid return of the F_{off} signal (Figure 6A and B). Interestingly, the voltage dependence of the F-V relationship is very similar for ($5.5_{/}5.5$) or ($7_{/}7$) conditions, while in ($7_{/}7$) the proton current appears at more negative voltages than the bulk of the fluorescence (Figure 6C). These results suggest that the voltage range of movement of the voltage sensor, as reported by the fluorescence of 201Anap, is dependent on the ΔpH, since the $V_{0.5}$ of the F-V is the same in pH_o/pH_i =$5.5_{/}5.5$, while the opening of the proton conduction pathway in pH_o/pH_i =$7_{/}7$, can occur after only a fraction of the voltage sensor movement has occurred and this coupling between voltage sensing and channel opening can be increased by low pH.

Discussion

In the experiments described here we have implemented patch-clamp fluorometry in combination with incorporation of a fluorescent non-canonical amino acid (NCAA) to study voltage-dependent gating in hH_V1 proton channels. Although voltage-clamp fluorometry (VCF) using TMRM has been used previously to study H_V1 channels (Qiu et al., 2013; Mony et al., 2015; Schladt and Berger, 2020), employing the fluorescent Anap NCAA has the advantages of being a smaller size probe and improving the specificity of fluorescence signals, since it is genetically encoded. The small size of Anap allowed us to incorporate the fluorophore into functional channels in several sites along the S4 and the S3-S4 loop. Since Anap was developed as an environmental sensitive probe, the fact that the emission spectrum of Anap in these sites is very similar to that of Anap in water, suggests that these residues are solvated in the native H_V1. The only position that shows a blue-shifted Anap spectrum is I202, which is the most C-terminal residue explored and might burry the Anap R-group in a more hydrophobic environment.

Since the activity of H_V1 proton channels can change the local concentration of protons near the conduction site and fluorescence probes have been used to detect these proton fluxes (De-la-Rosa et al., 2016; Zhang et al., 2016), we addressed whether Anap could change its fluorescence as a function of pH. We show that Anap is highly insensitive to pH in the range 4 to 8 and it does not change fluorescence in conditions in which high outward fluxes can change the local intracellular pH. Our experiments confirm that Anap can be used without interference from local changes in proton concentration.

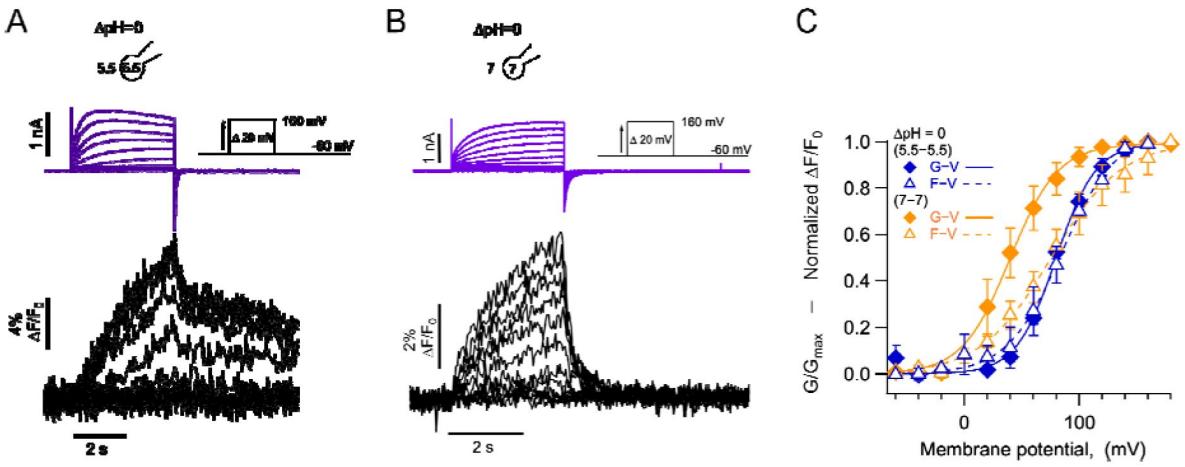

Figure 6.

Absolute pH values are gating determinants in hH_V1-1201Anap. A) Representative PCF experiment at ΔpH=0 (5.5_o-5.5_i). Currents are purple and fluorescence black. B) Similar experiment to A) with ΔpH=0 (7_o-7_i). Current and fluorescence traces color coded as in A). C) G-V (filled diamonds) and F-V (empty triangles) curves at ΔpH=0 but with different absolute pH values (pH_o/pH_i =5.5/5.5 in blue; pH_o/pH_i =7/7 in orange, n= 4). Boltzmann fit parameters were pH_o/pH_i =7/7 F-V: $V_{0.5}$= 75.3 ± 2.2 mV; q =0.8 ± 0.04 e_0. G-V: $V_{0.5}$= 39.6 ± 1.3 mV; q = 1.2 ± 0.1 e_0. pH_o/pH_i =5.5/5.5 F-V: $V_{0.5}$= 84.6 ± 2.1 mV; q =1.0 e_0 ± 0.1. G-V: $V_{0.5}$= 79.7 ± 1.8 mV; q = 1.4 ± 0.1 e_0. Data are mean ± s.e.m.

When incorporated at position 197, Anap produced fluorescence signals that indicate an increase in intensity with depolarization and saturated in magnitude at positive potentials. This behavior indicates dequenching of Anap as the S4 segments undergoes an outward movement during the activation conformational change. Anap has been incorporated in other membrane proteins, including the *Shaker* potassium channel, in which Anap was incorporated in the S4-S5 linker and displayed fluorescence quenching upon depolarization (Kalstrup and Blunck, 2018). Anap has been incorporated in the S4 of the hyperpolarization-activated cyclic nucleotide-gated (HCN) channel (Dai et al., 2019), where it is quenched or dequenched upon hyperpolarization in a position-dependent manner. It has also recently been incorporated at the bottom of the S4 in the voltage-dependent phosphatase, CiVSP (Mizutani et al., 2022), where it becomes quenched upon depolarization. The direction of the fluorescence changes due to S4 motion are difficult to predict, since, as we have shown, Anap's fluorescence can be affected by both the local environment's polarity and interaction with specific quenching groups that are part of the channel sequence.

The fluorescence changes we observe in 197Anap channels indicate that the G-V and F-V relationships have almost the same voltage-dependence at the ΔpH values tested, suggesting that S4 movement closely follows channel opening, and that S4 movement and activation of the proton conductance are equally affected by the proton gradient. A similar conclusion has been reached in studies measuring S4 movements of hH_V1 by fluorescence (Schladt and Berger, 2020) or in *Ciona* H_V1 by gating current recordings (Carmona et al., 2021). Interestingly, these changes in fluorescence as a function of voltage, are not accompanied by changes in the emission spectrum of Anap, suggesting that the probe remains in a solvated environment regardless of the state of the channel. This is in accordance with the finding that the VSD that forms hH_V1 channels has a large extracellular cavity able to contain many water molecules (Ramsey et al., 2010).

Since Anap remains solvated in the closed and open state, what is the origin of the reported fluorescence changes? As is common with other fluorescent probes, we hypothesized that an aromatic residue could act as an Anap quencher and thus found that an aromatic outside the S4 close enough to have this function is F150. Mutation F150A in the 197Anap background produced an increased Anap/mCherry fluorescence intensity as compared to 197Anap alone, indicating reduced quenching. This result suggests that 197Anap moves away from F150 as the S4 segment moves outward during channel activation. It should be noted that F150A-197Anap channels still produce fluorescence changes upon depolarization. This suggests that other amino acid residues apart from F150 (aromatic, charged) can also quench Anap or changes in Anap's quantum yield are still being produced by voltage-dependent solvent accessibility.

F150 has been shown to be part of a "hydrophobic gasket" through which S4 charges slide during channel activation. Mutations at this position and at W207 in the S4 produce altered gating (Banh et al., 2019; Cherny et al., 2015; Wu et al., 2022). In our case, F150A-197Anap shows a reduced shift of the G-V between ΔpH 0 and 1, from the expected ~40 mV to 22 mV, although the F-V curve shifts by 58 mV. These changes could be explained by altered movement of S4 through F150A, leading to changes in the coupling between voltage sensor movement and proton conductance activation. Also, this is the first time that F150 is reported as a possible actor in the pH-sensing mechanism of H_V1.

Substitution of 1201 for Anap allowed us to uncover a slow step in the deactivation pathway. The fluorescence signal observed upon channel closure by repolarization at ΔpH = 0 shows two components, one of which is much slower than channel closing as reported by the tail current. The fact that tail current is faster than the slow component of the deactivation fluorescence signal indicates that the latter is produced by a slow intermediate transition. This experimental observation is recapitulated by a simple kinetic model. Interestingly, recordings of gating currents in mutant *Ciona* H_V1 channels show that the charge return after depolarization can be very slow,

producing gating charge immobilization (Carmona et al., 2018). This observation of a singular slow transition in hH_V1 activation illustrates the value of fluorescence recording with a small probe such as Anap.

Our data thus far indicates that a fraction of S4 movement, as reported by the F-V relation, occurs before the increase of the proton conductance, and that S4 movement can continue after channel activation. Comparison of the V0.5 values of Q-V and G-V curves in hH_V1 channels (De La Rosa and Ramsey, 2018) indicates that charge moves at slightly more negative values than conductance, but not at all ΔpH values. Fluorescence changes depend on all the conformational states in which the fluorophore has distinct fluorescence values, while gating currents are produced during transitions between conformations with state-dependent charge distributions (Cha and Bezanilla, 1997). For these reasons, F-V and Q-V curves of multistate channels are not expected to be identical or contain the same information.

Our fluorescence data are consistent with recent experiments that have shown that the characteristic gating effect of the proton gradient on voltage-gated proton channels comes about by a conformational change that affects voltage sensor movement and not a channel opening transition happening after voltage-sensor activation. Furthermore, our modeling suggests that all transitions in the activation pathway, including a characteristic slow transition detected by fluorescence are modulated by ΔpH.

The mechanism of ΔpH modulation is still unknown. It has been proposed that the energy stored in the pH gradient is directly coupled to S4 movement to produce ΔpH-dependent gating (Carmona et al., 2021). We have previously proposed an allosteric model in which both extracellular and intracellular protons can affect local electrostatic networks and bring about ΔpH-gating (Rangel-Yescas et al., 2021). This class of models predicts the existence of multiple open states, which is supported by the observation that S4 movement can happen after channel opening.

A mechanism in which the proton gradient energy is coupled to S4 movement predicts that the absolute value of pH should not influence gating. Interestingly, we have observed that the absolute pH values used to set up a ΔpH = 0 do affect gating. When pH_o=5.5/pH_i=5.5, G-V and F-V are almost superimposed and the F_{off} signal has a fast and slow component; in contrast, when pH_o=7/pH_i=7, the F-V curve has almost the same voltage-dependence, but conductance can be observed at more negative voltages and the F_{off} signal only contains the fast component. These results suggest that the absolute pH in the extracellular side of the channel is a determinant of the steady-state gating, presumably modulating the slow rate constant in the activation pathway.

Materials and Methods

Molecular biology and HEK cell expression

A plasmid containing the human voltage-gated proton channel (hH_V1) was a gift from Dr. Ian Scott Ramsey (Virginia Commonwealth University, Richmond, VA). We used the fluorescent protein mCherry as a reporter to verify L-Anap incorporation. The construct hH_V1-mCherry was made by the PCR overlap technique, adding the sequence of fluorescent protein mCherry after the C-terminus of hH_V1 with the following linker sequence: $(Gly\text{-}Gly\text{-}Ser)_3$. This construct was subcloned into the pCDNA3.1 vector. For all hH_V1-TAG mutants, an amber codon (TAG) was introduced using appropriate mutagenic oligonucleotides and a protocol for whole plasmid site-directed mutagenesis employing KOD polymerase (Merck Millipore, Germany) as detailed in manufacturer's instructions and previous work (Zheng et al., 2004; Munteanu et al., 2012). The bacterial methylated DNA templates were digested with the DpnI restriction enzyme, and the mutant plasmids were confirmed by automatic sequencing at the Institute de Fisiología Celular, UNAM.

We used HEK293 cells for channel expression and L-Anap incorporation experiments. The HEK cells used in this study were found free of mycoplasma infection (Sigma-Aldrich mycoplasma detection kit). These cells were cotransfected with 0.1 - 1 μg of mutant hH_V1-TAG plasmid and 0.7 μg of pAnap plasmid (a gift from Dr. Sharona Gordon, University of Washington, Seattle, WA) using the transfection reagent JetPei (Polyplus-transfection). The pANAP plasmid contains the orthogonal pair tRNA/aminoacyl tRNA synthetase specific to L-Anap. The Methyl ester form of L-Anap; L-Anap-Me (AsisChem Inc.) was added to the medium of cells in 35 mm culture dishes from a storing stock solution of 10 mM to a final concentration of 10-20 μM. Through the text, we will refer to L-Anap as Anap for simplicity. Cells were incubated during 12-48 hours before experiments in Dulbecco's Modified Eagle Medium (DMEM, Invitrogen) supplemented with 10% fetal bovine serum (Invitrogen, USA) and penicillin-streptomycin (100 units/ml — 100 μg/ml, Invitrogen, USA) at 37 °C in a 5% CO_2 atmosphere. Around 4 hours before electrophysiological recordings, HEK293 cells were treated with 0.05% trypsin-ethylenediaminetetraacetic acid (Trypsin-EDTA) to obtain rounded cells, which were then re-platted in 35 mm glass-bottom dishes (World Precision Instruments, USA) and used for experiments within 3-6 hrs. All the experiments were performed at room temperature (~25°C).

Electrophysiology

Recordings of proton currents were performed in the whole-cell patch-clamp configuration using fire-polished borosilicate micropipettes (Sutter Instruments, USA). Currents were recorded by an Axoclamp 200B amplifier (Axon Instruments, USA) and acquired with an ITC-18 AD/DA converter (HEKA Elektronik, Germany), both controlled with Patchmaster software (HEKA Elektronik, Germany). Currents were low-passed filtered at 5 kHz and sampled at 20 kHz. The extracellular solution contained (in mM): 100 tetramethylammonium hydroxide and methanesulfonic acid (TMAOH-$HMESO_3$), 100 buffer ((2-(N-morpholino)ethanesulfonicacid (MES) for pH 5.5, and 6.0; 4-(2-hydroxyethyl)-1-piperazineethanesulfonic acid (HEPES) for pH 7.0 and 7.5), 2 $CaCl_2$, 2 $MgCl_2$, 8 HCl and pH-adjusted with TMAOH and HMESO. The intracellular solution contained (in mM): 80 (TMAOH-$HMESO_3$) 100 buffer (MES for pH 5.5 and 6.0; HEPES for pH 7.0 and 7.5), 10 ethylene glycol-bis(β-aminoethyl ether)-N,N,N',N'-tetraacetic acid (EGTA), 10 $MgCl_2$, and 4 HCl and pH-adjusted with TMAOH and HMESO. With these solutions, patch pipettes had a resistance of 2-5 MΩ. Since cells used in these experiments were round to improve space-clamp and currents were relatively small, no series-resistance compensation was employed. The voltage-clamp protocols varied depending on the value of ΔpH and are indicated in the figure legends. The interval between each test pulse was 45 s at the holding potential to facilitate return of slow fluorescence signals and minimize the effects of proton depletion.

Fluorescence measurements

Fluorescence measurements in whole-cell patch-clamp fluorometry (PCF) experiments were made using a TE-2000U (Nikon, Japan) inverted epifluorescence microscope with a 60x oil immersion objective (numerical aperture 1.4). A 405 nm solid-state laser (Compass 405-50 CW, COHERENT, USA) and a filter cube containing a 405/20-nm excitation filter, a 405-nm long pass dichroic mirror, and a 425-nm long-pass emission filter were used for Anap fluorescence excitation. For mCherry fluorescence, measurements were performed using an Ar-Ion laser (Spectra-Physics, Germany) and a filter cube with a 514/10-nm excitation filter, a 514-nm long pass dichroic mirror, and a 530-nm long-pass emission filter (Chroma, USA). Both lasers were through-air coupled, collimated using an optical cage system and appropriate optics (Thorlabs, USA) and then focused into the objective's back focal plane through the microscope's rear port. Imaging was performed using Luca or Ixon Ultra EMCCD cameras (Andor, Oxford instruments, Ireland) controlled by Micromanager software (Edelstein et al., 2014). The fluorescence of a region without cells was measured with the same ROI employed with cells and this background was subtracted from Anap fluorescence images. Image stacks from cells were recorded at 10-25 Hz (100 - 40 ms of exposure, respectively). To improve signal-to-noise ratio, 4×4 or 8×8 pixel binning was used. Initially,

fluorescence time course was measured from a region of interest (ROI) that included only the membrane of the patched cell. Identical results were obtained by using a ROI encompassing all the cell.

Fluorescence and proton current recording synchronization was achieved through a home-programed Arduino Uno microcontroller board (Arduino, Italy) triggered by a PatchMaster-generated TTL pulse.

For spectral measurements, the light from the microscope was collected by a SpectraPro 2150i imaging spectrograph (Princeton Instruments, USA) mounted between the microscope and EMCCD camera. The mCherry fluorescence was used as an indicator of membrane-associated channels. A small area from the membrane-associated mCherry fluorescence is selected using the spectrograph slit, and mCherry and Anap spectra were recorded by measuring a line scan 10 pixels wide from the cell membrane spectral image (Figure 2-Supplement 1). Background fluorescence spectrum was recorded from a region of the image without cells and subtracted from Anap and mCherry fluorescence. Unless indicated, all the spectra were obtained at resting potential in non-patched cells (Thomas and Smart, 2005a) and a ΔpH ~ −0.2.

Data analysis

IgorPro (Wavemetrics) and ImageJ (NIH) software were used to analyze the data. For the G-V relationships, conductance (G) was calculated from proton currents according to:

$$G(V) = \frac{I(V)}{V - V_{rev}}$$

Where V_{rev} is the proton current reversal potential, measured from the current-voltage relation. Then, G was normalized and fit to a Boltzmann function as follows:

$$\frac{G}{G_{max}} = \frac{1}{1 + \exp^{(q(V - V_{0.5})/K_B T)}}$$

Equation 1

Where q is the apparent gating charge (in elementary charges, e_0), V is the membrane potential, $V_{0.5}$ is the potential at which half of the maximal activation is reached, K_B is the Boltzmann constant and T is the temperature in Kelvin.

The time course of fluorescence in PCF experiments, was obtained from all the background-subtracted images in a stack (F_i), and the changes through time were normalized to the first image (F_0) as follows:

$$\frac{F_i - F_0}{F_0} = \frac{\Delta F}{F_0}$$

Then, this normalization was multiplied by 100 to obtain the percent change of fluorescence. This procedure was carried out for each stack at each voltage. The voltage-dependence of the fluorescence was estimated from F-V relationships. The value of the fluorescence at the end of the volage step was normalized and fit to a Boltzmann function:

$$\frac{F}{F_{max}} = \frac{1}{1 + \exp^{(q(V - V_{0.5})/K_B T)}}$$

Equation 2

Where F is the percent of fluorescence change at V potential and F_{max} is the maximum fluorescence percent change in each experiment at V potential. The meaning of q, V, $V_{0.5}$ and $K_B T$ is the same as in equation 1. All data are presented as the mean ± standard error of the mean (s.e.m.).

The time constants activation of proton currents and fluorescence signals were obtained by fitting of the second half of each trace to the equation:

$$I \text{ or } F(t) = A_{ss}\left(1 - e^{\left(-(t-t_o)/\tau\right)}\right)$$

Equation 3

Where A_{ss} is the amplitude of the fluorescent signal (F) or current (I) at steady state, τ is the time constant, and t_o is the time of start if the voltage pulse, both in ms. The voltage dependence of τ was calculated from a fit to equation:

$$\tau(V) = \tau(0) \cdot e^{\left(\frac{qV}{K_B T}\right)}$$

Equation 4

Where $\tau(0)$ is the activation time constant at 0 mV, q is the partial charge in e_0 units and V, K_B and T have the same meaning as in equation 1.

Modelling

Modelling of current and fluorescence was carried out using custom-written programs in IgorPro (Wavemetrics). The occupancy of each discreet state in the models was calculating by numerically solving the differential equations describing the transitions between states. The occupancy of each discreet state i is P_i and it was calculated by numerically solving the differential equations described by a master equation:

$$\frac{dP_i}{dt} = \sum_{i \neq j}(P_j k_{ji} - P_i k_{ij})$$

The rate constants k_{ij} or k_{ij} are given by:

$$k_{ij} = k_{ij}(0) \cdot \exp\left(-z_{ij} V / K_B T\right)$$

Where $k_{ij}(0)$ is the value of the rate constant at 0 mV, z_{ij} the partial charge associated with the transition and $K_B T$ have the same meaning as in Eq.1.

The current as a function of time tand voltage V was calculated as:

$$I(t,V) = \gamma_{ch} \cdot N \cdot (V - V_{rev}) \cdot P_o(t,V) + \gamma_{leak} \cdot (V - V_{rev}^{leak})$$

γ_{ch} is the single proton channel conductance, N is the number of channels, V_{rev} is the reversal potential and P_o is the probability of the open state. γ_{leak} is the leak conductance and V_{rev}^{leak} is the reversal potential of the leak currents.

The fluorescence was calculated as:

$$F(t,V) = \sum_{i=0}^{n} P_i\,(t,V) \cdot f_i$$

f_i is the fluorescence of the i-th state in arbitrary units.

Supporting information

Supplementary data

Acknowledgements

We thank Eduardo Guevara for measurements of Anap spectra in different solvents and Manuel Hernández for excellent technical support. We thank Dr. Sebastian Brauchi for the loan of the 405 nm laser. This work was supported by DGAPA-PAPIIT-UNAM grant No. IN215621. E. S-D is a doctoral student from Programa de Doctorado en Ciencias Bioquímicas-UNAM and was supported by a doctoral thesis scholarship from CONACyT No. 463819 (CVU 659182). M.E.O-C. is a doctoral student from Programa de Doctorado en Ciencias Biomédicas-UNAM and is supported by a doctoral thesis scholarship from CONACyT No. 788807 (CVU 1101710)

References

Banh R., Cherny V.V., Morgan D., Musset B., Thomas S., Kulleperuma K., Smith S.M.E., Pomès R., DeCoursey T.E. (2019) **Hydrophobic gasket mutation produces gating pore currents in closed human voltage-gated proton channels** *Proc. Natl. Acad. Sci. U.S.A* **116**:18951–18961 https://doi.org/10.1073/pnas.1905462116 | Google Scholar

Carmona E.M., Fernandez M., Alvear-Arias J.J., Neely A., Larsson H.P., Alvarez O., Garate J.A., Latorre R., Gonzalez C. (2021) **The voltage sensor is responsible for ΔpH dependence in H v 1 channels** *Proc. Natl. Acad. Sci. U.S.A* **118**:e2025556118 https://doi.org/10.1073/pnas.2025556118 | Google Scholar

Carmona E.M., Larsson H.P., Neely A., Alvarez O., Latorre R., Gonzalez C. (2018) **Gating charge displacement in a monomeric voltage-gated proton (H v 1) channel** *Proc. Natl. Acad. Sci. U.S.A* **115**:9240–9245 https://doi.org/10.1073/pnas.1809705115 | Google Scholar

Catacuzzeno L., Franciolini F. (2022) **The 70-year search for the voltage sensing mechanism of ion channels** *The Journal of Physiology* :JP282780 https://doi.org/10.1113/JP282780 | Google Scholar

Cha A., Bezanilla F. (1997) **Characterizing Voltage-Dependent Conformational Changes in the K Channel with Fluorescence** *Neuron* **19**:1127–1140 https://doi.org/10.1016/S0896-6273(00)80403-1 | Google Scholar

Cha A., Bezanilla F. (1998) **Structural Implications of Fluorescence Quenching in the Shaker K+ Channel** *Journal of General Physiology* **112**:391–408 https://doi.org/10.1085/jgp.112.4.391 | Google Scholar

Chatterjee A., Guo J., Lee H.S., Schultz P.G. (2013) **A Genetically Encoded Fluorescent Probe in Mammalian Cells. J** *Am. Chem. Soc* **135**:12540–12543 https://doi.org/10.1021/ja4059553 | Google Scholar

Cherny V.V., Markin V.S., DeCoursey T.E. (1995) **The voltage-activated hydrogen ion conductance in rat alveolar epithelial cells is determined by the pH gradient** *The Journal of general physiology* **105**:861–896 Google Scholar

Cherny V.V., Morgan D., Musset B., Chaves G., Smith S.M.E., DeCoursey T.E. (2015) **Tryptophan 207 is crucial to the unique properties of the human voltage-gated proton channel, hHV1** *Journal of General Physiology* **146**:343–356 https://doi.org/10.1085/jgp.201511456 | Google Scholar

Cowgill J., Chanda B. (2019) **The contribution of voltage clamp fluorometry to the understanding of channel and transporter mechanisms** *Journal of General Physiology* **151**:1163–1172 https://doi.org/10.1085/jgp.201912372 | Google Scholar

Dai G., Aman T.K., DiMaio F., Zagotta W.N. (2019) **The HCN channel voltage sensor undergoes a large downward motion during hyperpolarization** *Nat Struct Mol Biol* **26**:686–694 https://doi.org/10.1038/s41594-019-0259-1 | Google Scholar

De La Rosa V., Ramsey I.S. (2018) **Gating Currents in the HV1 Proton Channel** *Biophysical Journal* **114**:2844–2854 https://doi.org/10.1016/j.bpj.2018.04.049 | Google Scholar

De-la-Rosa V., Suárez-Delgado E., Rangel-Yescas G.E., Islas L.D. (2016) **Currents through HV1 channels deplete protons in their vicinity** *Journal of General Physiology* **147**:127–136 https://doi.org/10.1085/jgp.201511496 | Google Scholar

Eckert R., Sibaoka T. (1968) **The Flash-Triggering Action Potential of the Luminescent Dinoflagellate Noctiluca** *Journal of General Physiology* **52**:258–282 https://doi.org/10.1085/jgp.52.2.258 | Google Scholar

Edelstein A.D., Tsuchida M.A., Amodaj N., Pinkard H., Vale R.D., Stuurman N. (2014) **Advanced methods of microscope control using μManager software** *J Biol Methods* **1**:e10 https://doi.org/10.14440/jbm.2014.36 | Google Scholar

Gonzalez C., Contreras G.F., Peyser A., Larsson P., Neely A., Latorre R. (2012) **Voltage sensor of ion channels and enzymes** *Biophys Rev* **4**:1–15 https://doi.org/10.1007/s12551-011-0061-8 | Google Scholar

Gordon S.E., Munari M., Zagotta W.N. (2018) **Visualizing conformational dynamics of proteins in solution and at the cell membrane** *eLife* **7**:e37248 https://doi.org/10.7554/eLife.37248 | Google Scholar

Hondares E., Brown M.A., Musset B., Morgan D., Cherny V.V., Taubert C., Bhamrah M.K., Coe D., Marelli-Berg F., Gribben J.G., Dyer M.J.S., DeCoursey T.E., Capasso M. (2014) **Enhanced activation of an amino-terminally truncated isoform of the voltage-gated proton channel HVCN1 enriched in malignant B cells** *Proc. Natl. Acad. Sci. U.S.A* **111**:18078–18083 https://doi.org/10.1073/pnas.1411390111 | Google Scholar

Hong L., Pathak M.M., Kim I.H., Ta D., Tombola F. (2013) **Voltage-sensing domain of voltage-gated proton channel HV1 shares mechanism of block with pore domains** *Neuron* **77**:274–287 Google Scholar

Islas L.D., Zagotta W.N. (2006) **Short-range Molecular Rearrangements in Ion Channels Detected by Tryptophan Quenching of Bimane Fluorescence** *Journal of General Physiology* **128**:337–346 https://doi.org/10.1085/jgp.200609556 | Google Scholar

Kalstrup T., Blunck R. (2013) **Dynamics of internal pore opening in K v channels probed by a fluorescent unnatural amino acid** *Proc. Natl. Acad. Sci. U.S.A* **110**:8272–8277 https://doi.org/10.1073/pnas.1220398110 | Google Scholar

Kalstrup T., Blunck R. (2018) **S4-S5 linker movement during activation and inactivation in voltage-gated K+ channels** *Proc. Natl. Acad. Sci. U.S.A* **115** https://doi.org/10.1073/pnas.1719105115 | Google Scholar

Klymchenko A.S. (2017) **Solvatochromic and Fluorogenic Dyes as Environment-Sensitive Probes: Design and Biological Applications** *Acc. Chem. Res* **50**:366–375 https://doi.org/10.1021/acs.accounts.6b00517 | Google Scholar

Koch H.P., Kurokawa T., Okochi Y., Sasaki M., Okamura Y., Larsson H.P. (2008) **Multimeric nature of voltage-gated proton channels** *Proc. Natl. Acad. Sci. U.S.A* **105**:9111–9116 https://doi.org/10.1073/pnas.0801553105 | Google Scholar

Kusch J., Zifarelli G. (2014a) **Patch-Clamp Fluorometry: Electrophysiology meets Fluorescence** *Biophysical Journal* **106**:1250–1257 https://doi.org/10.1016/j.bpj.2014.02.006 | Google Scholar

Kusch J., Zifarelli G. (2014b) **Patch-Clamp Fluorometry: Electrophysiology meets Fluorescence** *Biophysical Journal* **106**:1250–1257 https://doi.org/10.1016/j.bpj.2014.02.006 | Google Scholar

Lee S.-Y., Letts J.A., MacKinnon R. (2008) **Dimeric subunit stoichiometry of the human voltage-dependent proton channel HV1** *Proc. Natl. Acad. Sci. U.S.A* **105**:7692–7695 https://doi.org/10.1073/pnas.0803277105 | Google Scholar

Li Q., Shen R., Treger J.S., Wanderling S.S., Milewski W., Siwowska K., Bezanilla F., Perozo E. (2015) **Resting state of the human proton channel dimer in a lipid bilayer** *Proc. Natl. Acad. Sci. U.S.A* :112 https://doi.org/10.1073/pnas.1515043112 | Google Scholar

Lishko P.V., Kirichok Y. (2010) **The role of HV1 and CatSper channels in sperm activation: HV1 and CatSper channels in sperm activation** *The Journal of Physiology* **588**:4667–4672 https://doi.org/10.1113/jphysiol.2010.194142 | Google Scholar

Ma J., Gao X., Li Y., DeCoursey T.E., Shull G.E., Wang H. (2022) **The HVCN1 voltage-gated proton channel contributes to pH regulation in canine ventricular myocytes** *The Journal of Physiology* **600**:2089–2103 https://doi.org/10.1113/JP282126 | Google Scholar

Mizutani N., Kawanabe A., Jinno Y., Narita H., Yonezawa T., Nakagawa A., Okamura Y. (2022) **Interaction between S4 and the phosphatase domain mediates electrochemical coupling in voltage-sensing phosphatase (VSP)** *Proc. Natl. Acad. Sci. U.S.A* **119**:e22 https://doi.org/10.1073/pnas.2200364119 | Google Scholar

Mony L., Berger T.K., Isacoff E.Y. (2015) **A specialized molecular motion opens the HV1 voltage-gated proton channel** *Nat Struct Mol Biol* **22**:283–290 https://doi.org/10.1038/nsmb.2978 | Google Scholar

Munteanu B., Braun M., Boonrod K. (2012) **Improvement of PCR reaction conditions for site-directed mutagenesis of big plasmids** *J. Zhejiang Univ. Sci. B* **13**:244–247 https://doi.org/10.1631/jzus.B1100180 | Google Scholar

Musset B., Cherny V.V., Morgan D., Okamura Y., Ramsey I.S., Clapham D.E., DeCoursey T.E. (2008) **Detailed comparison of expressed and native voltage-gated proton channel currents: Voltage-dependent proton channel gating** *The Journal of Physiology* **586**:2477–2486 https://doi.org/10.1113/jphysiol.2007.149427 | Google Scholar

Pantazis A., Olcese R. (2012) **Relative transmembrane segment rearrangements during BK channel activation resolved by structurally assigned fluorophore-quencher pairing** *Journal of General Physiology* **140**:207–218 https://doi.org/10.1085/jgp.201210807 | Google Scholar

Puljung M.C. (2021) **ANAP: A versatile, fluorescent probe of ion channel gating and regulation** In: *In Methods in Enzymology* Elsevier pp. 49–84 Google Scholar

Qiu F., Rebolledo S., Gonzalez C., Larsson H.P. (2013) **Subunit Interactions during Cooperative Opening of Voltage-Gated Proton Channels** *Neuron* **77**:288–298 https://doi.org/10.1016/j.neuron.2012.12.021 | Google Scholar

Ramsey I.S., Mokrab Y., Carvacho I., Sands Z.A., Sansom M.S.P., Clapham D.E. (2010) **An aqueous H+ permeation pathway in the voltage-gated proton channel HV1** *Nat Struct Mol Biol* **17**:869–875 https://doi.org/10.1038/nsmb.1826 | Google Scholar

Ramsey I.S., Moran M.M., Chong J.A., Clapham D.E. (2006) **A voltage-gated proton-selective channel lacking the pore domain** *Nature* **440**:1213–1216 https://doi.org/10.1038/nature04700 | Google Scholar

Ramsey I.S., Ruchti E., Kaczmarek J.S., Clapham D.E. (2009) **HV1 proton channels are required for high-level NADPH oxidase-dependent superoxide production during the phagocyte respiratory burst** *Proc. Natl. Acad. Sci. U.S.A* **106**:7642–7647 https://doi.org/10.1073/pnas.0902761106 | Google Scholar

Randolph A.L., Mokrab Y., Bennett A.L., Sansom M.S., Ramsey I.S. (2016) **Proton currents constrain structural models of voltage sensor activation** *eLife* **5**:e18017 https://doi.org/10.7554/eLife.18017 | Google Scholar

Rangel-Yescas G., Cervantes C., Cervantes-Rocha M.A., Suárez-Delgado E., Banaszak A.T., Maldonado E., Ramsey I.S., Rosenbaum T., Islas L.D. (2021) **Discovery and characterization of HV1-type proton channels in reef-building corals** *eLife* **10**:e69248 https://doi.org/10.7554/eLife.69248 | Google Scholar

Sasaki M., Takagi M., Okamura Y. (2006) **A Voltage Sensor-Domain Protein Is a VoltageGated Proton Channel** *Science* **312**:589–592 https://doi.org/10.1126/science.1122352 | Google Scholar

Schladt T.M., Berger T.K. (2020) **Voltage and pH difference across the membrane control the S4 voltage-sensor motion of the HV1 proton channel** *Sci Rep* **10**:21293 https://doi.org/10.1038/s41598-020-77986-z | Google Scholar

Shaner N.C., Campbell R.E., Steinbach P.A., Giepmans B.N.G., Palmer A.E., Tsien R.Y. (2004) **Improved monomeric red, orange and yellow fluorescent proteins derived from Discosoma sp. red fluorescent protein** *Nat Biotechnol* **22**:1567–1572 https://doi.org/10.1038/nbt1037 | Google Scholar

Smith S.M.E., Morgan D., Musset B., Cherny V.V., Place A.R., Hastings J.W., DeCoursey T.E. (2011) **Voltage-gated proton channel in a dinoflagellate** *Proc. Natl. Acad. Sci. U.S.A* **108**:18162–18167 https://doi.org/10.1073/pnas.1115405108 | Google Scholar

Stefani E., Ottolia M., Noceti F., Olcese R., Wallner M., Latorre R., Toro L. (1997) **Voltage-controlled gating in a large conductance Ca 2+-sensitive K+ channel (hslo)** *Proc. Natl. Acad. Sci. U.S.A* **94**:5427–5431 https://doi.org/10.1073/pnas.94.10.5427 | Google Scholar

Tao X., Lee A., Limapichat W., Dougherty D.A., MacKinnon R. (2010) **A Gating Charge Transfer Center in Voltage Sensors** *Science* **328**:67–73 https://doi.org/10.1126/science.1185954 | Google Scholar

Taylor A.R., Chrachri A., Wheeler G., Goddard H., Brownlee C. (2011) **A Voltage-Gated H+ Channel Underlying pH Homeostasis in Calcifying Coccolithophores** *PLoS Biol* **9**:e1001085 https://doi.org/10.1371/journal.pbio.1001085 | Google Scholar

Thomas P., Smart T.G. (2005a) **HEK293 cell line: A vehicle for the expression of recombinant proteins** *Journal of Pharmacological and Toxicological Methods* **51**:187–200 https://doi.org/10.1016/j.vascn.2004.08.014 | Google Scholar

Thomas P., Smart T.G. (2005b) **HEK293 cell line: A vehicle for the expression of recombinant proteins** *Journal of Pharmacological and Toxicological Methods* **51**:187–200 https://doi.org/10.1016/j.vascn.2004.08.014 | Google Scholar

Tombola F., Ulbrich M.H., Isacoff E.Y. (2008) **The Voltage-Gated Proton Channel HV1 Has Two Pores, Each Controlled by One Voltage Sensor** *Neuron* **58**:546–556 https://doi.org/10.1016/j.neuron.2008.03.026 | Google Scholar

Vaid M., Claydon T.W., Rezazadeh S., Fedida D. (2008) **Voltage Clamp Fluorimetry Reveals a Novel Outer Pore Instability in a Mammalian Voltage-gated Potassium Channel** *Journal of General Physiology* **132**:209–222 https://doi.org/10.1085/jgp.200809978 | Google Scholar

Villalba-Galea C.A. (2014) **HV1 proton channel opening is preceded by a voltage-independent transition** *Biophysical journal* **107**:1564–1572 Google Scholar

Wang Y., Li S.J., Wu X., Che Y., Li Q. (2012) **Clinicopathological and Biological Significance of Human Voltage-gated Proton Channel HV1 Protein Overexpression in Breast Cancer** *Journal of Biological Chemistry* **287**:13877–13888 https://doi.org/10.1074/jbc.M112.345280 | Google Scholar

Wu L.-J. (2014) **Microglial Voltage-Gated Proton Channel HV1 in Ischemic Stroke** *Transl. Stroke Res* **5**:99–108 https://doi.org/10.1007/s12975-013-0289-7 | Google Scholar

Wu X., Zhang L., Hong L. (2022) **The role of Phe150 in human voltage-gated proton channel** *iScience* **25** https://doi.org/10.1016/j.isci.2022.105420 | Google Scholar

Young V.C., Artigas P. (2021) **Displacement of the Na + /K+ pump's transmembrane domains demonstrates conserved conformational changes in P-type 2 ATPases** *Proc. Natl. Acad. Sci. U.S.A* **118**:e2019317118 https://doi.org/10.1073/pnas.2019317118 | Google Scholar

Yu Y., Luo X., Li C., Ding F., Wang M., Xie M., Yu Z., Ransom B.R., Wang W. (2020) **Microglial HV1 proton channels promote white matter injuries after chronic hypoperfusion in mice** *J. Neurochem* **152**:350–367 https://doi.org/10.1111/jnc.14925 | Google Scholar

Zhang L., Bellve K., Fogarty K., Kobertz W.R. (2016) **Fluorescent Visualization of Cellular Proton Fluxes** *Cell Chemical Biology* **23**:1449–1457 https://doi.org/10.1016/j.chembiol.2016.10.013 | Google Scholar

Zhang Q., Ren Y., Mo Y., Guo P., Liao P., Luo Y., Mu J., Chen Z., Zhang Y., Li Y., Yang L., Liao D., Fu J., Shen J., Huang W., Xu X., Guo Y., Mei L., Zuo Y., Liu J., Yang H., Jiang R. (2022) **Inhibiting HV1 channel in peripheral sensory neurons attenuates chronic inflammatory pain and opioid side effects** *Cell Res* **32**:461–476 https://doi.org/10.1038/s41422-022-00616-y | Google Scholar

Zhao C., Tombola F. (2021) **Voltage-gated proton channels from fungi highlight role of peripheral regions in channel activation** *Commun Biol* **4**:261 https://doi.org/10.1038/s42003-021-01792-0 | Google Scholar

Zhao R., Kennedy K., De Blas G.A., Orta G., Pavarotti M.A., Arias R.J., de la Vega-Beltrán J.L., Li Q., Dai H., Perozo E., Mayorga L.S., Darszon A., Goldstein S.A.N. (2018) **Role of human HV1 channels in sperm capacitation and white blood cell respiratory burst established by a designed peptide inhibitor** *Proc. Natl. Acad. Sci. U.S.A* **115** https://doi.org/10.1073/pnas.1816189115 | Google Scholar

Zheng L., Baumann U., Reymond J.-L. (2004) **An efficient one-step site-directed and site-saturation mutagenesis protocol** *Nucleic Acids Research* **32**:e115 https://doi.org/10.1093/nar/gnh110 | Google Scholar

Author information

Esteban Suárez-Delgado
Department of Physiology, School of Medicine, UNAM, Mexico City,04510, Mexico, Department of Biology, Xenon Pharmaceuticals Inc., 3650 Gilmore Way, Burnaby, BC V5G 4W8, Canada
ORCID iD: 0000-0003-0147-3451

M. E. Orozco-Contreras
Department of Physiology, School of Medicine, UNAM, Mexico City,04510, Mexico

Gisela E. Rangel-Yescas
Department of Physiology, School of Medicine, UNAM, Mexico City,04510, Mexico
ORCID iD: 0000-0003-2766-6040

León D. Islas
Department of Physiology, School of Medicine, UNAM, Mexico City,04510, Mexico
ORCID iD: 0000-0002-7461-5214

Correspondence to: León D. Islas, Department of Physiology, School of Medicine, Universidad Nacional Autónoma de México (UNAM), Circuito Escolar S/N, Ciudad Universitaria, Ciudad de México, 04510, México, leon.islas@gmail.com

Copyright

Authors' response (28 November 2022)

> ***GENERAL ASSESSMENT***
>
> *This interesting preprint by Suárez-Delgado et al. explores the mechanism by which activation of the Hv1 voltage-activated proton channel is dependent upon both the voltage and pH difference across the membrane. The authors are the first to incorporate the fluorescent unnatural amino acid, Anap, into the extracellular regions of the S4 helix of human Hv1 to monitor transitions of S4 upon changes in voltage or pH. The authors first checked that Anap is pH insensitive for practical use in Hv1, where changes in local pH are known to occur when the voltage sensor activates and the proton pore opens. Anap was incorporated at positions throughout the S3-S4 linker and the extracellular end of S4 (up to the 202nd residue) of hHv1 and some positions showed clear voltage-dependent changes in fluorescence intensity. The authors also obtained fluorescence spectra at different voltages and observed no spectral shifts, raising the possibility that voltage dependent changes in fluorescence intensity could primarily be due to*

> *fluorescence quenching. Upon mutation of F150, the Anap signal at the resting membrane voltage increased, suggesting dequenching upon removal of F150. The authors also discovered that the kinetics of Anap fluorescence upon membrane repolarization have two phases (rapid and slow) under certain pH conditions and that there is a pH-dependent negative shift of the conductance-voltage (G-V) relation compared with the fluorescence-voltage (F-V) relation in some mutants. The biphasic kinetics of the fluorescence decay upon repolarization were explained by modelling a slower transition of return from intermediate resting state to a resting state. The pH-dependent shift of the G-V relation from the F-V relation provides insight into mechanisms of ΔpH-dependent gating of Hv1, a longstanding enigma. Overall, the approaches are rigorous, the figures show important results, and this work paves the way for the use of Anap fluorescence to study Hv1 gating and modulation.*

We thank the reviewers for the careful reading and assessment of our manuscript and for the constructive criticism. We have tried to respond to all the essential revisions, both by rewriting sections and performing some experiments or new analysis. Below we respond one by one to all the points raised. Please also note that we have added an author to the manuscript, who has carried out new experiments included in this revised version of the preprint.

> ***RECOMMENDATIONS***
>
> ***Revisions essential for endorsement:***
>
> 1. *In its current form, the narrative of the preprint has two threads. One on the mechanisms of Anap fluorescence changes (mainly quenching) and another on a previously unappreciated transition of the voltage sensor, as revealed by Anap. Our impression is that the preprint suffers somewhat from this split focus, which could be resolved by explaining why Anap was used to explore voltage sensor activation in Hv1 in the introduction. Perhaps the authors could also explain the advantage of smaller sized fluorophores compared to other maleimide-based fluorophores earlier in the introduction, or the utility of being able to insert Anap into transmembrane segments. The authors should more clearly point out how they exploited the advantages of Anap as a tool in this study. It would furthermore be helpful to discuss previous studies using nongenetic tools for VCF and spell out how they have delineated key aspects of Hv1, which would help to emphasize how several positions studied here (for example, 201 and 202) could not be labelled with cysteine-based fluorophores.*

We think that this is a very useful suggestion and we have expanded the introduction to more pointedly indicate the contributions of previous voltage-clamp fluorometry experiments in Hv1 channels and to clearly explain why we chose to pursue the use of a genetically-encoded small fluorophore such as Anap.

> 1. *We think the authors should be cautious about understanding the physicochemical nature of Anap using prodan as a model. It would be helpful to discuss the possibility that undetected spectral shifts due to a nonquenching mechanism could be overlooked, even though major signal changes can be explained by fluorescence quenching in their data. Regarding the mechanisms of remaining voltage-dependent fluorescence changes of F150A-A197Anap, it would be helpful for the authors to suggest possible ideas about which residues might account for remaining signals.*
>
>   *The beautiful spectral data for Anap is impressive. However, the physicochemical basis of the fluorescence change of Anap cannot be understood by simple extension of findings for prodan, which shows structural similarity to Anap. Our understanding is that changes*

> *in Anap fluorescence can only reveal a change in the structural relationship between Anap and one of its neighbors because the physicochemical basis of Anap fluorescence is complicated. For example, fluorescence could also be affected by the electrostatic environment, stretch of peptide bond, etc. Previous studies, including those of TRP channels, showed that the kind of environmental changes that Anap faces in ion channels do not necessarily induce large spectral shifts, unlike in cell-free spectral analyses using distinct solvents. Further, only minor shifts in spectra occur upon local structural change, as seen in previous work including Xu et al. Nat. Commun. 2020 11:3790. Such minor shifts could be perhaps overlooked even when Anap is incorporated into S4 and exposed to environmental change. Therefore, it is not easy to decode the physicochemical basis of Anap fluorescence changes. F150A-A197Anap has increased fluorescence and no change in spectral pattern, leading the authors to conclude that F150 quenches Anap fluorescence of A197 position. However, a significant amount of fluorescence change still occurs upon changes in membrane potential after F150 is changed to alanine (Figure 4). It is very likely that quenching is not the only mechanism underlying the observed voltage induced change of Anap fluorescence of Hv1. The authors suggest that remaining voltage-dependent fluorescence change of F150A-A197Anap could be due to interaction with other aromatic residues, but this has not been tested.*

Thank you for pointing out our oversimplified discussion of the mechanisms of Anap fluorescence changes in Hv1 channels. We have taken into account your comments and present a more nuanced and toned-down discussion of the possible mechanisms at play in our experimental system.

> *1. The current version of the preprint is missing important control experiments, ideally performed using western blots to measure protein expression or, if that is not possible, proton current and fluorescence measurements, to demonstrate that protein expression or functional channels are not seen for all mutants in the absence of ANAP (but in the presence of the tRNA and Rs construct). A similar control for imaging would be to use ANAP alone without encoding.*

We thank the reviewers for this recommendation. We show that the number of cells showing mCherry fluorescence is greatly diminished in the absence of L-Anap, but in the presence of the tRNA and synthetase. As suggested, we have included results of control experiments in which we attempted to record currents from cells expressing the constructs: F150A-A197tag, Q191tag, A197tag and L201tag co-expressed with the tRNA and synthetase-coding plasmid (pANAP) and in the absence of L-Anap. We struggled to find red fluorescing cells and recorded currents from a relatively small number of these cells, most of which was leak current. We now include these data in Figure 1-Supplement 1B. These control experiments show that there is very little leakage of expression of channels that did not incorporate Anap.

> *1. Aromatics in the S4 segment were ruled out as potential quenchers on the assumption that they would move together with Anap during gating. It should be noted, however, that Hv1 is a dimer and therefore a fluorophore attached to S4 in one subunit could be quenched by S4 aromatics in the neighboring subunit if were close to the dimer interface. In Fujiwara et al. J. Gen. Physiol. 2014 143:377-386, for example, W207 does not appear very far from labeled positions in the adjacent S4. This possibility should be mentioned in the discussion.*

We appreciate the reviewers' concern regarding the role of other aromatic residues near Anap incorporation sites, especially the ones close to the subunit interface given that Hv1 is a dimer. We now mention the possibility that other residues could be quenching groups,

especially given the fact that some quenching remains in the double mutant F150A-A197Anap (line 272 in results and line 432 in discussion). We have also included a new analysis of the ratio of Anap/mCherry fluorescence (at resting membrane potential) for all insertion sites. This shows a decreased ratio as Anap gets inserted in residues closer to the c-terminus of S4, which is evidence of a quenching group located near the center of the transmembrane domains (Figure 4-Supplement 1).

> *1. It is not clear whether the Anap spectra purely represent Hv1 incorporated into the plasma membrane or perhaps include signals from the cytoplasm or channels in internal membranes (whether assembled or incompletely assembled). It would be helpful to provide a more complete presentation of the data obtained and to provide more information in the Methods Section. In the Methods section, it is stated "The spectra of both fluorophores (Anap and mCherry) were recorded by measuring line scans of the spectral image of the cell membrane, and the background fluorescence from a region of the image without cells was subtracted". How are signals from cell membranes specified in this method being discriminated from those associated with the cytoplasm and intracellular membranes? If spectral data include signals from free Anap in the cytoplasm or Hv1 in intracellular membranes, spectral shifts upon membrane potential changes will be difficult to detect, even when Anap is incorporated into Hv1 and senses environmental change by voltage-induced conformational change. In Figure 3E, wavelength spectra were shown as standardized signals for different voltages. Amplitude change would be demonstrated (spectrum at different voltages without standardization should be shown).*

We appreciate the concern related to the origin of the fluorescence signals and we have improved both the presentation and the associated figures. Since this is also a concern for the experiments that determined the pH-dependence of Anap incorporated at position Q191, we have included a figure supplement 1 to Figure 2 in which we explain how the membrane was visualized. We use mCherry fluoresce as an indication of plasma membrane-associated channels, since its red fluorescence is easier to detect in the membrane than Anap fluorescence (even though cytoplasm dialysis in whole-cell should diminish the amount of free Anap, it is difficult to distinguish Anap fluorescence in the membrane by itself). Once the membrane associated mCherry fluorescence is detected, the measurement of the spectrum from a very small membrane area is insured because the spectrograph slit delimits light collection to a very small vertical area and the horizontal line scan further limits light measurement. These procedures are now made explicit in methods section and supplementary figure mentioned before. Moreover, we explain that they were also followed in experiments where the cell was under voltage-clamp. The spectral data in Figure 3E is now presented without normalization to show the voltage-dependent change in amplitude without changes in peak emission wavelength.

> *In Figure 4, spectra were compared between A197Anap and F150A-A197Anap, showing increases of fluorescence in F150A-A197Anap. Was this signal measured at resting membrane potential? How does the spectrum change when the membrane potential is changed?*

As in the experiments of figure 1E, the spectra were obtained in non-patched cells. Thus, the signal was measured at the HEK cell resting potential (~ -30 mV) and a $\Delta pH \approx 0.2$. We have now incorporated that information in the methods section and the figure description. On the other hand, we did not perform experiments measuring the double mutant spectra at different voltage steps, so we cannot respond to the second question.

> *Rationales for the confirmation of signals originating from the cell surface for Hv1 Anap might include the observations that: a) some mutants showed slightly different spectral*

> *patterns (in particular, Q191Anap showed a small hump at longer wavelengths, which is proposed to represent FRET between mCherry and Anap) and b) signal intensity was voltage dependent (if signals originate from endomembranes, they should not be voltage dependent). Mentioning these two points earlier in the text might help to alleviate concerns about the location of the protein that contributes to the measured signals.*

These are great suggestions and we have incorporated them to the text (lines 156, 190 and 216 Results section), along with a better explanation of procedures followed to measure mostly membrane-associated fluorescence (see new Figure 2-Supplement 1).

> *1. In Fig 5, the fluorescence kinetics do not really match the current activation kinetics for panels A, B, and C. Is there an explanation for this mismatch? It would be helpful to have the fitted data in the figure. A more thorough comparison of the kinetics of currents and fluorescence would be helpful throughout the study.*

We believe that the kinetics of fluorescence and current does not match because the current activation rate is overestimated due to a small amount of proton depletion present in recordings from large currents. This is an unavoidable problem in proton current recordings, even with the high concentration of proton buffer used in our experiments and the long time-intervals between each voltage pulse. For this reason, we did not undertake a systematic exploration of kinetics. Nonetheless, the current and fluorescence rates are very close and have the same voltage dependence, indicating a close correlation between voltage-sensor movement and current activation. We now explain this limitation in the manuscript text (line 223 and 327, results section).

> *1. Which construct of hHv1 was used to obtain the data in Figure 6? Unless we missed it, this information is not provided in the text or figure legend. Is it for L201Anap? This figure also shows an intriguing finding that the G-V relationship is negatively shifted from the F-V relationship at pHo7-pHi7 but not at pHo5.5-pHi5.5. A shifted G-V relation with the same ΔpH contrasts with what has been reported in other papers. However, the authors did not really discuss this surprising finding in the light of previous references. Could the shift of the G-V relation between two pH conditions with the same ΔpH be due to any position-specific effect of Anap? If Figure 6 represents L201Anap mutant, the presence of Anap at L201 probably makes such shift of G-V curve in Figure 6C? The authors should openly discuss this finding in relation to what has been reported in the literature.*

Yes, construct L201Anap was used in Figure 6. This is stated now in the figure legend and in the corresponding main text. We agree that the leftward shift of the GV with respect to the FV in pHi7-pHo7 is an intriguing finding, suggesting that coupling between S4 movement and proton permeation can be regulated by the absolute value of the pH. We discuss this in the results section. The DeCoursey group has shown evidence in W207 mutants of hHv1 that the absolute value of pH can modulate the voltage dependence of the conductance. Although we had mentioned these results, we now mention them more prominently and also discuss the possibility that this might be a unique feature of introducing Anap at L201.

> *1. The authors suggest that the small hump near 600 nm in Figure 1E represents FRET between Anap and mCherry. It is surprising that FRET can take place across the membrane. Can the authors point to another case of FRET taking place across a cell membrane? One possibility might be that misfolded proteins place mCherry and Anap close to each other. It is also curious that only A191Anap did not show such a FRET-like signal. Also, if there is FRET, why wouldn't this also contribute to the voltage-dependent changes in fluorescence?*

We thank the reviewers for bringing up this point. Based on published data, we assumed that mCherry could not be excited by 405 nm radiation, thus our conclusion that the observed emission near 604 nm is FRET between Anap and mCherry. We have now measured the excitation of the Hv1-mCherry construct and observe that the 405 nm laser is capable of exciting mCherry and produced ~2 % emission (as compared to 514 nm excitation), which is almost the same as that observed for the Hv1Anap-mCherry channels. We now conclude that the second hump in the emission spectrum near 600 nm is due to direct excitation of mCherry.

On the other hand, FRET across the membrane has been demonstrated for the membrane-bound hydrophobic anion dipicrylamine and membrane-anchored GFP (Chanda, et al. A hybrid approach to measuring electrical activity in genetically specified neurons. *Nature neuroscience*, 2005, vol. 8, no 11, p. 1619-1626.) and dipicrylamine and GFP in the c-terminus of CNG channels (Taraska & Zagotta, Structural dynamics in the gating ring of cyclic nucleotide–gated ion channels. *Nature structural & molecular biology*, 2007, vol. 14, no 9, p. 854). Finally, single-molecule FRET between dyes placed extracellularly and intracellularly in Hv1 channels has been demonstrated (Han et al. eLife 2022;11:e73093. DOI: https:// doi. org/ 10. 7554/ eLife. 73093).

A191Anap shows the hump at ~600 nm, but we think it's less evident because Anap at 191 is less quenched (see Figure 4-Supplement 1 and answer to point 4 above).

> 1. *F150A-A197Anap shows a leftward shift of the F-V relation compared with the G-V relation only when ΔpH=1. Another unusual finding with F150A-A197Anap is the very small shift of the G-V relation between ΔpH=0 and ΔpH=1, when other reports in the literature suggest it should be 40 mV or more. Are these peculiar properties simply due to the absence of Phe at position 150, which might play a critical role in gating as one of the hydrophobic plugs of Hv1? To address this possibility, it would be ideal to compare different ΔpH values with and without F150 when Anap is incorporated at a different position (such as L201Anap). Regardless, it would be helpful to discuss this point.*

We now discuss these changes in the discussion (lines 440-446).

> 1. *In Figure 1E, I202Anap exhibits a blue shift in its spectrum suggesting the environment of Anap on I202 is more hydrophobic than the other sites. We presume these spectra were obtained at a negative membrane voltage, but the text or legend should clearly state how these were obtained. The authors should also explain whether the whole cell or edge was imaged. If these are at negative membrane voltages, might the Anap spectrum shift to higher wavelengths (i.e. more hydrophilic) when the membrane is depolarized? Did the authors find any spectral shift for I202Anap when doing a similar test as depicted in Figure 3E?*

Yes, the spectrum of I202Anap was obtained at the resting potential (~ -30 mV), as were all spectra in Figure 1E. We now indicate this clearly in the methods section and in the figure legend. Fluorescence was measured from the membrane region as indicated by mCherry fluorescence and as illustrated in Figure 2-Supplement 1. We did not explore this mutant further and we cannot answer the question of whether a depolarizing potential might produce a red shift of the spectrum.

> 1. *In Figure 3E, spectra are shown as normalized signals for different voltages, but an amplitude change should also be demonstrated by providing raw spectra at different voltages.*

We have changed figure 3E to show non-normalized data that now show the increase in fluorescence intensity and no wavelength shift in the fluorescence spectrum of Anap (see also response to point 5).

> 1. *In Figure 4, spectra are compared between A197Anap and F150A-A197Anap, showing increase of fluorescence in F150A-A197Anap. Were these obtained at a negative membrane voltage? How do these spectra change when membrane potential is changed?*

See response to point 4 of "Revisions essential for endorsement" section.

> ***Additional suggestions for the authors to consider:***
>
> 1. *The authors propose that Anap fluorescence tracks an S4 movement involved in the opening of the channel. They also argue that the existence of more than one open state could explain why the increase in florescence upon depolarization lags the proton current in most cases. While they convincingly show that Anap is not pH sensitive per se, when incorporated into the protein, the fluorescence efficiency of the fluorophore could still be affected by protonation of channel residues in the immediate environment when the channel opens, even after S4 has completed its movement. To address this alternative explanation, the authors could use Hv1 mutants with strongly reduced proton conductance. Channels bearing mutations corresponding to N214R or D112N were used successfully to isolate Hv1 gating currents from the much larger proton currents (De La Rosa & Ramsey, Biophys. J. 2018 114:2844-2854; Carmona et al. PNAS 2018 115:9240-9245; Carmona et al. PNAS 2021 118: e2025556118). Perhaps, they could be used with patch clamp fluorometry as well?*

This is an interesting suggestion that could be explored in a follow up study.

> 1. *The data showing that Hv1-197Anap is quenched by Phe at position 150 are very nice. Yet, it would be useful to show that the quenching is specific to F150 using a negative control. F149, for instance, is just next to F150 but points in a different direction, so its mutation to alanine should not affect Hv1-197Anap fluorescence.*

This is an interesting suggestion, but, as suggested by reviewers, we think there is a possibility that other aromatic residues could contribute to quenching. Given the absence of a reliable structure for Hv1, prediction of the relative positions of any resides is very difficult and thus we did not attempt the suggested experiment.

> 1. *A major finding of this work is the identification of a slow kinetic component that is highly sensitive to ΔpH. Earlier studies found that the ability of Hv1 to sense ΔpH is altered by some channel modifications, e.g., in the loop between TMH2 and TMH3 (Cherny et al. J. Gen. Physiol. 2018 150:851-862). Did the authors check whether any of these modifications alter the transition responsible for the slow kinetic component? For instance, a suppression of the transition resulting from a H168X mutation would help tighten the link to ΔpH sensing.*

We did not carry out any of these experiments.

> 1. *We understand that it is difficult to tightly control intracellular and extracellular pH when Hv1 is heterologously expressed in mammalian cells. The G-V relation is not always reliable because accumulation of protons or depletion of protons upon Hv channel activity will alter gating, as the authors have previously published (De La Rosa et al., J. Gen. Physiol. 2016 147:127-136). Could the kinetic analysis of Anap fluorescence be affected by similar alterations to proton concentration in the vicinity of Hv1? It would be helpful for the authors to comment on this specifically.*

Thanks for this suggestion. Yes, we think that the kinetics, specially of ionic currents can be affected by even small changes in the pH gradient, for this reason we did not attempt a systematic kinetic analysis. We mention this in the text where we compare the voltage dependence of current and fluorescence activation for construct A197Anap (line 223).

> 1. *Quenching of Anap by Phe could be verified in cell free conditions using a spectrophotometer with different concentrations of Phe, or citing the literature if it has already been reported.*

We attempted this experiment but were unsuccessful in observing Anap quenching by phenylalanine at the concentrations of phenylalanine that can be attained in aqueous solution. We suspect that Phe quenching of Anap could happen by electron transfer or ground-state complex formation, in which case near proximity is necessary and higher concentrations of Phe would be required to detect quenching in solution. However, we measured the absorbance of Anap in the absence and presence of phenylalanine (Phe) (and tyrosine (Tyr)) at the concentrations that can be achieved in aqueous solution (8 mM and 1mM, respectively). Absorbance measurements can detect ground-state complex formation even at relatively low concentrations (J.R. Lakowicz, 1999, Principles of Fluorescence Spectroscopy). We observed that the absorbance of Anap is modified by the presence of Tyr or Phe, indicating that these amino acids indeed interact with Anap, possibly through ground-state complex formation. We include this data for the reviewers to inspect.

> 1. *The authors did not cite any example of Anap incorporation into S4 helices, but there are several recent papers where Anap was utilized to probe motion of S4 in other channels. Examples include Dai et al., Nat. Commun. 2021 12:2802 and Mizutani et al. PNAS 2022 119:e2200364119.*

Thanks for this observation, we have included these important results in the discussion.

> 1. *In the Anap-free negative control (with only A197TAG plasmid transfection), the mCherry signal seems positive (Supplementary Figure 1, left row, second from the top). Is this due to unexpected skipping of the TAG codon to make mCherry-containing partial polypeptides? It would seem like an explanation is needed.*

Thanks for bringing this up. We do not know the exact origin of these leak expression of red fluorescence. We think that, as suggested, there is a possibility that skipping of the Amber codon can lead to a methionine at the end of S4 acting as a second translation initiation site, giving rise to truncated channels that would express mCherry but not currents. This is consistent with the fact that we cannot detect currents in the absence of Anap but we see a small number of red cells.

> 1. *The data of Figure 3E are shown as data with different membrane voltages. But there is no information about membrane voltage for Fig. 1E and Fig. 2A and Fig. 4B. Are these from unpatched cells? Please clarify.*

See response to point 4 of "Revisions essential for endorsement" section.

> 1. *G-V relations are shown for F150A-A197Anap, but current traces of F150A-A197Anap are missing.*

We have modified the figure to include current and fluorescence traces.

> 1. *On Page 11, Line 303 says "experimental F-V relationship is positively shifted by 10 mV with respect to the G-V curve". But looking at the data Fig5D, the shift at ΔpH=2 seems the opposite. Perhaps "positively" should be "negatively" in this sentence?*

Thanks for pointing out this mistake. We have found that this misunderstanding was provoked because of a mistake with the image labeling of F-V and G-V curves for the ΔpH=2 data, we have now corrected the figure. The shift of F-V is indeed positive to G-V as stated before.

(This is a response to peer review conducted by Biophysics Colab on version 1 of this preprint.)